Enhancing RHex Robot Performance with Innovative Bioplastic Legs Responsive to Humidity

Yi Zhao

CMU-RI-TR-23-79

Dec 20, 2023

The Robotics Institute
School of Computer Science
Carnegie Mellon University
Pittsburgh, PA

Thesis Committee:
Zeynep Temel, *Chair*
Aaron Johnson
Uksang Yoo

Submitted in partial fulfillment of the requirements for the degree of Master of Science in Robotics.

I love robots.

Abstract

Designing and developing robots that can effectively navigate real-world environments poses a significant challenge. To overcome this, many robotic systems draw inspiration from the adaptive behaviors of animals, which have evolved to thrive in diverse surroundings. Amphibious animals, for instance, seamlessly transition between walking and swimming, optimizing their locomotion efficiency based on environmental cues. However, existing robots often face limitations in adapting to their surroundings, hindering their applications in crucial domains such as land and water search and rescue, natural disaster inspection, and environmental monitoring.

This thesis seeks to contribute valuable insights into the enhancement of robot capabilities for applications demanding flexibility and efficiency in diverse, dynamic environments, and to address the aforementioned challenge by introducing innovative, stimuli-responsive robot legs made from bioplastic material onto a pre-existing low-cost, small-scale RHex robot system. These bioplastic legs enable the robot to dynamically adjust leg stiffness in response to environmental humidity levels, presenting a versatile solution for navigating various terrains. In the following thesis, we explored the material development, fabrication techniques, and manufacturing processes involved in creating the humidity-responsive robot legs. Following this, we also presented characteristic analysis of the bioplastic legs to explore their responsiveness to different durations of exposure to varying humidity levels. Finally, to evaluate the practical impact of humidity-responsive legs, four robot experiments were conducted to assess the RHex robot's performance across different terrains. The results of these experiments demonstrate the advantages of humidity-responsive legs, showcasing their adaptability to specific terrains and environmental conditions.

Acknowledgments

I would like to express my deepest gratitude to my thesis advisor, Zeynep Temel, for her unwavering support, invaluable guidance, and scholarly insights throughout the entire research process. Her expertise, patience, and encouragement have been instrumental in shaping this thesis and fostering my academic growth.

I am also grateful to the members of my thesis committee, Aaron Johnson and Uksang Yoo, for their constructive feedback and thoughtful suggestions that significantly enhanced the quality of this work.

I extend my appreciation to the Robot Institute at Carnegie Mellon University for providing a conducive academic environment and access to resources that facilitated my research endeavors.

Special thanks go to my family and friends for their understanding, encouragement, and strong belief in my abilities. Their emotional support has been a constant source of strength and motivation.

This thesis represents the culmination of a challenging yet rewarding journey, and the support I have received from those mentioned above has been invaluable. Thank you all for being an integral part of this academic endeavor.

Contents

When this dissertation is viewed as a PDF, the page header is a link to this Table of Contents.

List of Figures

List of Tables

Chapter 1

Introduction

1.1 Motivation

In the real world, the environment changes all the time – rain, snow, sunlight... These environmental changes are all factors that can change the behavior of animals [36]. Amphibious animals, for example, are able to change between walking and swimming quickly with respect to the environment around them, maximizing their locomotion efficiency. However, most robots tend to have difficulties adapting to these changes, resulting in either the need for manual help or the loss of efficiency and effectiveness during the long adjustment period.

When performing tasks in the real world, the environment always plays a key role in influencing robot performance. In addition, many robots in real-world situations, especially small robots, are required to traverse difficult terrains to search and rescue people or provide reconnaissance in harsh environments. Thus, it is paramount in academic research to explore methods of making robots better adapt to environmental changes and sustain high efficiency and effectiveness while in these environments.

Wheeled robots are commonly used in the field of contemporary robotics for their simple design, low cost, and easy-to-control locomotion. However, when faced with varying and difficult terrain requirements (e.g. stones, uneven, or muddy) or environments with extremely low or high friction, wheeled robots usually fail to maintain effectiveness due to their lack of adaptability.

RHex robot is a kind of unique hexapod robot known for its unique C-shaped

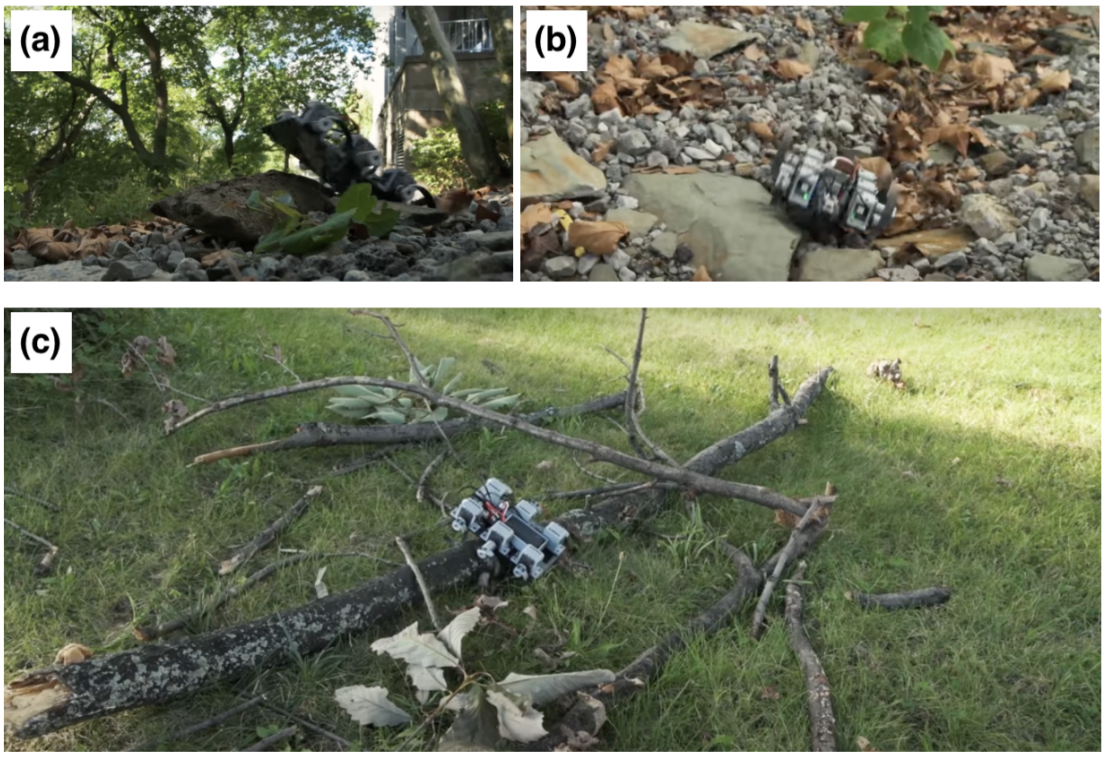

Figure 1.1: RHex in nature overcoming rough terrains. (a) MiniRHex across big rock (Image Source: Ackerman article). (b) MiniRHex across rocks and leaves (Image Source: Ackerman article). (c) MiniRHex across tree branches (Image Source: Ackerman article).

leg design and renowned for its agility and versatility [41]. It is able to overcome some of the rough terrain issues, like traversing through sand, rocks, and roots [1], shown in Figure 1.1 a-c. Some variants of the RHex robot were also designed to swim underwater, AQUA [17], for example. These abilities provide a significant advantage over the previously mentioned wheeled robots in terms of environment and terrain adaptability. However, despite these advantages, RHex robots still suffer from traction issues in humid environments, where the surface conditions may become slippery enough for the legs to lose traction and for the robot to get stuck [40].

1.2 Problem Definition

MiniRHex robot, a close design variation of the RHex robot, is a small, open-source, fully programmable, and cost-efficient hexapod robot [1, 3]. Currently, little research has been conducted on how the materials of the MiniRhex robot legs could impact the performance of the robot, especially while treading through wet terrain or environments with high humidity variations.

To fill in this gap, this thesis focuses on the utilization of an innovative bio-plastic material [32] to improve the performance of the MiniRHex robot in high humidity environments. Inspired by tree frogs' ability to adapt to both dry and wet environments, we designed new legs for MiniRHex using bioplastic which allows the legs and surface of the legs to change their stiffness and traction characteristics with respect to humidity. This capability of the material opens up new possibilities for the development of MiniRHex robots that respond rapidly to changes in their surroundings, especially in wet or slippery conditions.

1.3 Relevant Works

1.3.1 Small-scale Robots

The development and application of small-scale robots have garnered significant attention within the field of robotics [18]. Nowadays, small-scale robots are used in plenty of areas. For the purposes of this study, we will consider small-scale robots as robots that are less than the characteristic volume of 0.004 cubic meters. Small-scale robots can reach places where larger robots cannot [26], observe and monitor the environment without attracting attention from wildlife [14], and perform high precision and small invasion operations in medical applications [42]. Additionally, they are able to be carried around easily for transportation, are able to act together and form a swarm, are easier to manufacture, and are more cost effective for experiments or education purposes [26]. Small-scale robots have been widely used in the industry to perform a large variety of tasks. In human related applications, they have been used to provide invasive medical procedures [5, 23], search and rescue operation, and navigating narrow disaster areas and finding survivors [31, 38]. In agricultural

applications, they have been used for planting, harvesting, and environmental monitoring [8, 30, 45]. In space exploration, they are commonly used due to their smaller size (easy transportation) and low energy cost (easier to be powered up with solar power in space where electricity is extremely limited) [22, 26]. In marine application, they are also commonly used for exploring and mapping underwater environments, studying marine life without panicking them, and inspecting narrow and hard to access infrastructures, such as pipelines [48].

1.3.2 Bio-inspired Locomotion on Small-scaled Robots

Small-scale robots have various locomotion types that are specifically designed to suit the applications areas illustrated previously, including walking with legs or wheels, crawling, jumping, and swimming [19]. A big portion of small-scale robots are bio-inspired, since animals, after millions of years evolution, naturally have developed efficient locomotion patterns based on their species and body structures. Take tree frogs, for example. In wet environments, the mucus channels on their toe pads play a crucial role in providing traction by funneling away excess fluid on wet surfaces. In arid environments, these mucus channels create surface tension on dry or uneven surfaces and allow the tree frog to grasp well [21, 24]. Another example is the octopus, which is an inspiration for many stiffness-tuning robots. The octopus arm utilize a combination of transverse and longitudinal muscle contractions, allows for versatile movements such as shortening, bending, and stiffening with antagonistic co-contractions [10]. Similar to the octopus, various other animals, including fish, worms, and snakes, also adjust stiffness through muscle compression and release.

Amphibious animals, like salamanders, showcase flexible limb structures enabling them to walk on land by coordinating diagonal limbs and swim in water by folding back the limbs and propagating axial undulations from head to tail [11]. In fact, animals that have tunable stiffness in locomotion inspire the locomotion design and development in a lot of small-scale robots, including stability for quadruped robots traversing uneven terrains [51], octopus inspired robot arms control [10, 27, 28, 33], snake robot locomotion [20], worm robot locomotion [7], fish-like robot for efficient swimming [52], venus fly trap to vary stiffness through bistable structure [53], human foot inspired robot foot for adapting diverse terrains [39], salamander-like swimming

and walking amphibious robot [11], and cockroach inspired miniRHex robot for difficult terrains and large obstacles [15].

1.3.3 Stiffness Tuning Methods

The stiffness tuning methods in robotics can be divided into two main categories: interaction between structural elements and the property of material [13].

One method of interaction between structural elements is by jamming [28]. Imagine a bag of beans was sealed and is vacuumed. The bag of beans is soft and malleable when there is air in the bag, but becomes stiffer after it is vacuumed. Aside from the direct vacuum based jamming, there are also other jamming methods such as passive variable jamming [43], layer jamming [44], tubular jamming [37]. They are all using power, force, or pressure to adjust the interaction between particles in the robot to achieve tunable stiffness. This method is widely used and simple to implement. However, its implementation usually requires large and heavy materials and mechanical components [13], and therefore is rarely used in small-scaled mobile robots.

Another way of interacting between the structural elements is the antagonistic method [13]. This method was inspired by the muscles of animals [10]. For example, when you are pulling an object, the muscles are sticking out towards the skin, and the arm becomes stiffer. This method allows very fast response times and can generally be implemented with lightweight components, but is generally difficult to easily control with any degree of precision [13].

The other stiffness tuning method is to utilize the property of materials to achieve controlled stiffness changes. Most of the previous work has investigated the melting point of alloys and polymers to achieve a phase change of the material, thus achieving a state of tunable stiffness [13]. Low melting point alloy (LMPA) is widely used as components for stiffness tuning in robotics due to its ability to switch to the liquid state at a relatively low temperature (42°C-70°C) and to achieve around 3.5 times difference in stiffness [49]. LMPA is also able to achieve local stiffness tuning using localized and selective heating [13]. Another commonly used material is polymer. A polymer material's shear modulus would change with temperature and result in glass transition, a reversible transition that could change the material from a hard and

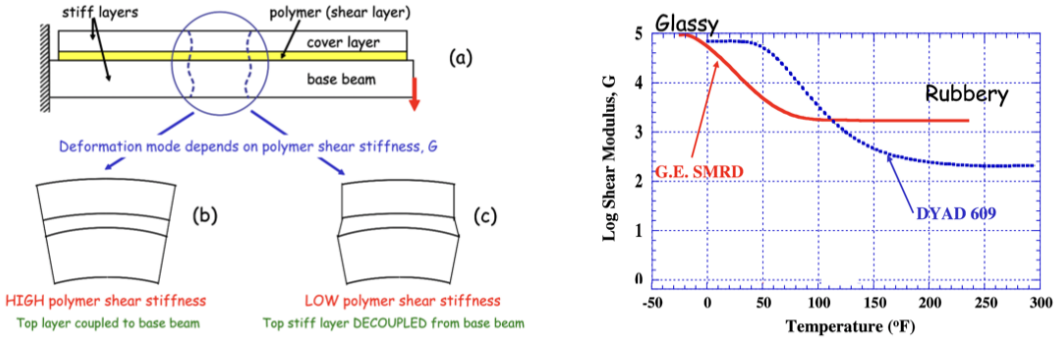

Figure 1.2: Two figures from research by F Gandhi and S-G Kang, showing the behavior of glass transition of polymer and how it was used in their stiffness changing system. Left: Schematic representation of a multi-layered beam, and deformation modes corresponding to high and low polymer shear moduli (Image Source: Gandhi1 and Kang (2007)). Right: Typical variation in the polymer shear modulus with increase in temperature (Image Source: Gandhi1 and Kang (2007)).

"glass" like state to a softer and rubbery state [16]. An example of this is shown in Figure 1.2. Other materials were also experimented with and studied for tunable stiffness, such as shape memory polymers [35], bulk polymer [2], gallium [7], stimuli-responsive polymer nanocomposites [6], and self-healing wax-coated composites [9]. In addition, research on the combinations of methods was also conducted, such as octopus inspired robot which utilizes LMPA with the antagonistic method mentioned previously [10], innovative thermoplastic variable stiffness composites with networked sensing and control [34], and hybrid multi-material 3D Printing with shape memory polymer layer [50]. Most of the material rigidity tuning strategies have large stiffness changing range and are able to be attached to small-scaled robots, but they also have limitations on response velocity, low energy transduction efficiency, and potential safety vulnerability posed by thermal distribution.

From these works, we note that in order to achieve controlled stiffness tuning and use them in small-scale applications, the commonly utilized method is to use material properties and apply external stimuli. We also note that the predominant stiffness tuning methods based on material properties typically utilize power or heat as external stimuli for active stiffness tuning, and have not encountered any research where the tuning stimuli are derived from passive sources, such as environmental factors like humidity.

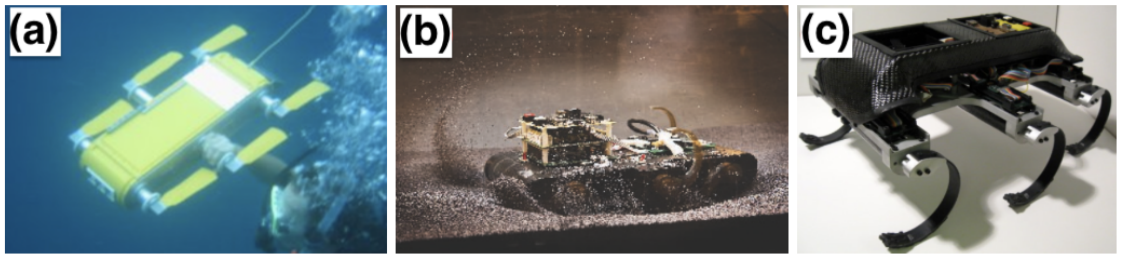

Figure 1.3: Variations of RHex robot. (a) AQUA, an underwater robot (Image Source: E. Milios (2004)). (b) SandBot (Image Source: Koditschek (2009)). (c) EduBot (Image Source: Komsuoglu (2010)).

1.3.4 MiniRHex and Environment

RHex/MiniRHex robot is the inspiration of many other robots, such as the underwater robot AQUA, which is able to navigate in water using paddle legs [17], SandBot, which is a smaller robot that was designed to march on sand [12, 29], and EduBot, which is a smaller robot that adopts the RHex's locomotion strategy and is widely used in classrooms [15, 25], see Figure 1.3. The original RHex (X-RHex) robot is very expensive, while the MiniRHex robot is a smaller version of it with less cost, which is designed to meet the need for experiment and education purposes. The MiniRhex is easy to assemble, and very cost effective — only about $200 compared to the large X-RHex which is $20,000 [3].

The locomotion of MiniRhex robot is based on walking with 6 C-shaped legs. When it's walking, there are always 3 legs in contact with the ground and 3 in the air — one from the middle of one side and two from the non-middle of another side. These legs rotate and alternate to allow the robot to move, as shown in Figure 1.4 a-d.

Previous research has shown that locomotor dynamics are independent from body mass but depend on gait and leg number. They mentioned that the relative stiffness per leg was similar for all animals and appears to be a very conservative quantity in the design of legged locomotor systems [4]. Based on this research, we suspect that the stiffness of the legs of the MiniRHex robot plays a role in its locomotion ability. Moreover, another research has shown that increasing the stiffness of the legs has a positive impact on the performance of EduBot on grass [15]. This also shows that

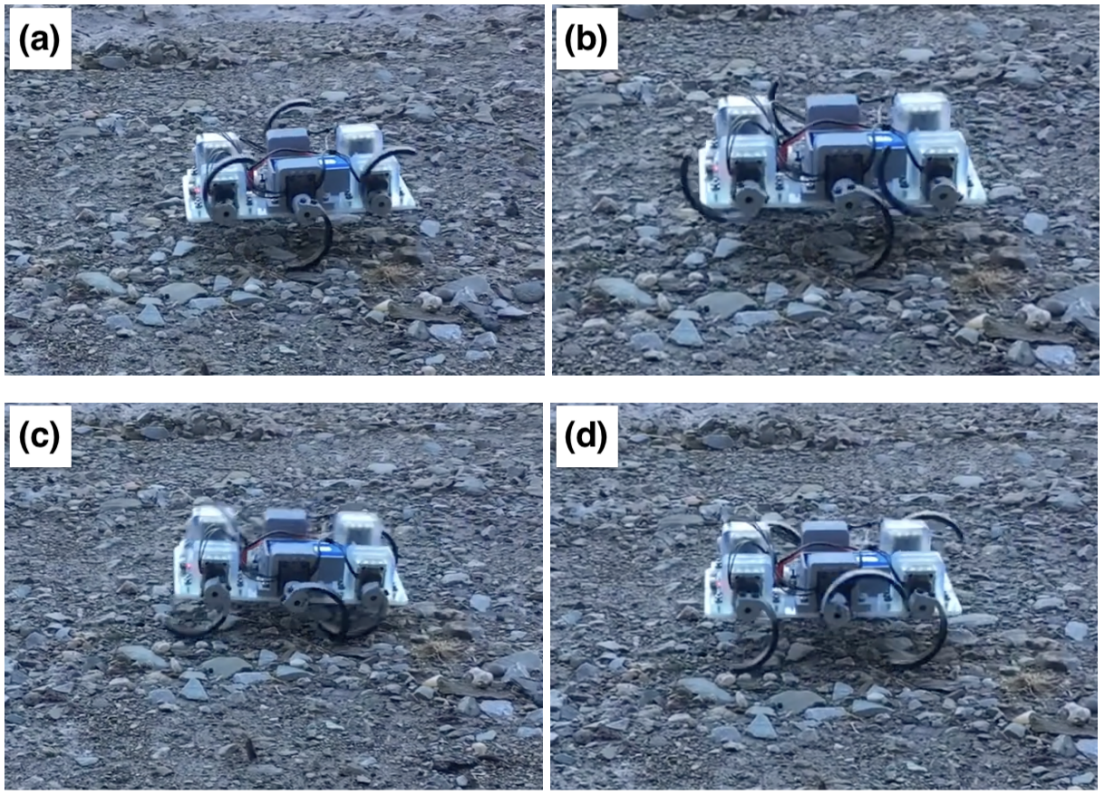

Figure 1.4: Figures showing how MiniRHex is alternating its legs when walking, ordered from (a) to (d). (Image Source: Dynamic Walking Conference (2018)).

the stiffness of the legs of MiniRHex robots significantly affect their performance.

1.4 Thesis Outline

To illustrate the composition of this new humidity-responsive leg design, we will detail the process of material development, exploration of fabrication techniques with bioplastic and the process for fabrication of legs, including lamination of thin sheets of bioplastic and new curing method with molding (Chapter 2). We also conducted characterization experiments with the legs, including a stability test to understand the repeatability of experimenting with the leg and force displacement test to understand how the bioplastic leg responds to different durations of exposure to environmental humidity levels (Chapter 3). Moreover, we explored two small-scaled robots for

attaching the bioplastic legs (TinyRHex and MiniRHex) and included the methods to attach the legs on the robots accordingly (Chapter 3). Finally, to gauge the impact of humidity-responsive legs on the Rhex robot's performance across different humidity environments (high environmental humidity, submerged, etc) and terrains (incline, wet, soft foam, etc), we conducted four experiments: friction coefficient test, incline test, foam test, and aqua test. (Chapter 4)

Chapter 2

Material Development, Fabrication, and Manufacturing

Bioplastic was originally developed for medical purposes. In one of the potential medical use cases, a specific type of bioplastic, similar to polyethylene terephthalate (PET) when dry and seaweed when wet, was made into a sheet that could be folded into a small pill using origami techniques [32]. The medicine is supposed to be enclosed in the bioplastic origami folding, and the goal is to have the bioplastic folding reach the stomach, where it should be able to react with the water in the body and expand in the stomach. Should this be successful, it would supposedly make the medicine stay in the patient's stomach for a longer release duration. Inspired by this potential use case, this thesis explored the use cases in the robotics field regarding the material's ability to change stiffness when reacting with water. In the following sections, two fabrication techniques are explained: lamination of thin sheets of bioplastic (section 2.1) and a new curing method with molding (section 2.2).

2.1 Fabrication Technique: Lamination

In this section, the lamination technique [46] that uses more compliant materials laminated between rigid materials is explored and revised with materials capable of stiffness-tuning (i.e. bioplastic). The laminate technique was applied with the top and bottom layers as a specific rigid material (e.g. cardboard, FR4) and the

middle compliant layer as bioplastic. Additionally, two adhesive layers are intersected between the rigid layers and the compliant layer to bind them firmly. This resulted in a 5-ply composite lamination material in sheet form (with layers being rigid - adhesive - compliant - adhesive - rigid in order).

This lamination technique explored here originates from a fabrication process called Smart Composite Microstructures (SCM) [46]. SCM was designed for creating small-scale robots that use novel composite materials, and offers a cheaper, quicker, and superior method for rapid prototyping by integrating rigid links and large-angle flexure joints through a combination of laser micromachining and lamination.

Inspired by the SCM technique, various materials for the top/bottom rigid link layers and the middle compliant layer are explored and tested for lamination. Initially, prototypes with 0.53 mm cardboard as the rigid link layer and 0.1 mm plastic as the compliant layer were made to test the fabrication process. After extensive testing, the optimal length for the flexure joints (i.e. gap between the two laminated rigid links) is derived to follow the below formula:

gap_{opt}: optimal flexure joint length

l_{rigid}: rigid layer thickness

l_{adhsv}: adhesive layer thickness

l_{cmpl}: compliant layer thickness

$$gap_{opt} = \sqrt{2} * (l_{rigid} + l_{adhsv} + 0.5 * l_{cmpl})$$

This gap is long enough to allow for 90 degree bending of the rigid layer, but not too long to cause over-bending as the cardboard layers contact each other (see Figure 2.1).

After prototyping to find the flexure joint length (i.e. the gap between the laminates), the plastic (compliant layer) is replaced with bioplastic sheet to allow for changes in stiffness with respect to humidity exposure. The same formula above is applied to calculate the required thickness of bioplastic sheet:

$$gap_{bioplastic} = \sqrt{2} * (0.53mm + 0.15mm + 0.5 * 0.16mm) = 1.07mm$$

Following these parameters, the laminated material is produced in a 4-step process (section 2.1.1 - section 2.1.4).

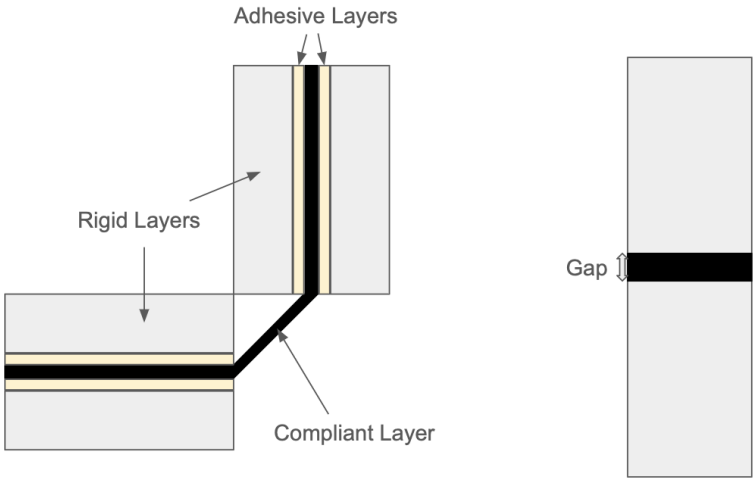

Figure 2.1: 5-ply composite lamination rigid layers (grey), adhesive layers (yellow), and compliant layer (black). Left: side view of the laminated piece with layers labeled. Right: front view of the laminated piece with the gap for the exposure of the compliant layer.

2.1.1 Step 1 Preparation

Prepare thin dowel pins that could be used for lamination, as shown in Figure 2.2 a - b. Prepare an acrylic board (see Figure 2.2 c) that measures 280 mm long, 160 mm wide, and 5 mm thick. Laser cut 96 1.473 mm diameter holes on the board as shown in Figure 2.2 c such that the holes are evenly spaced in a 20 mm square grid pattern. Ensure that the hole diameter is slightly smaller than the dowel pin diameter to allow insertion with tightness.

2.1.2 Step 2 Cutting the Layers

First, locate the rigid material sheet on the laser cutter and cut out the top and bottom layers following the shape in Figure 2.3 a. Remove all the materials, including the cutout pieces. Then, put the adhesive layer sheet and cut out two adhesive layers also using Figure 2.3 a. Take the two cutout pieces and locate them on the table with the non-adhesive paper side facing the table. Remove everything from the laser cutter, and place the bioplastic sheet on the laser cutter. Proceed to laser cut the shape in Figure 2.3 b. Remove everything from the laser cutter again and clean up all the leftover pieces in the laser cutter. Then, put another rigid material sheet on

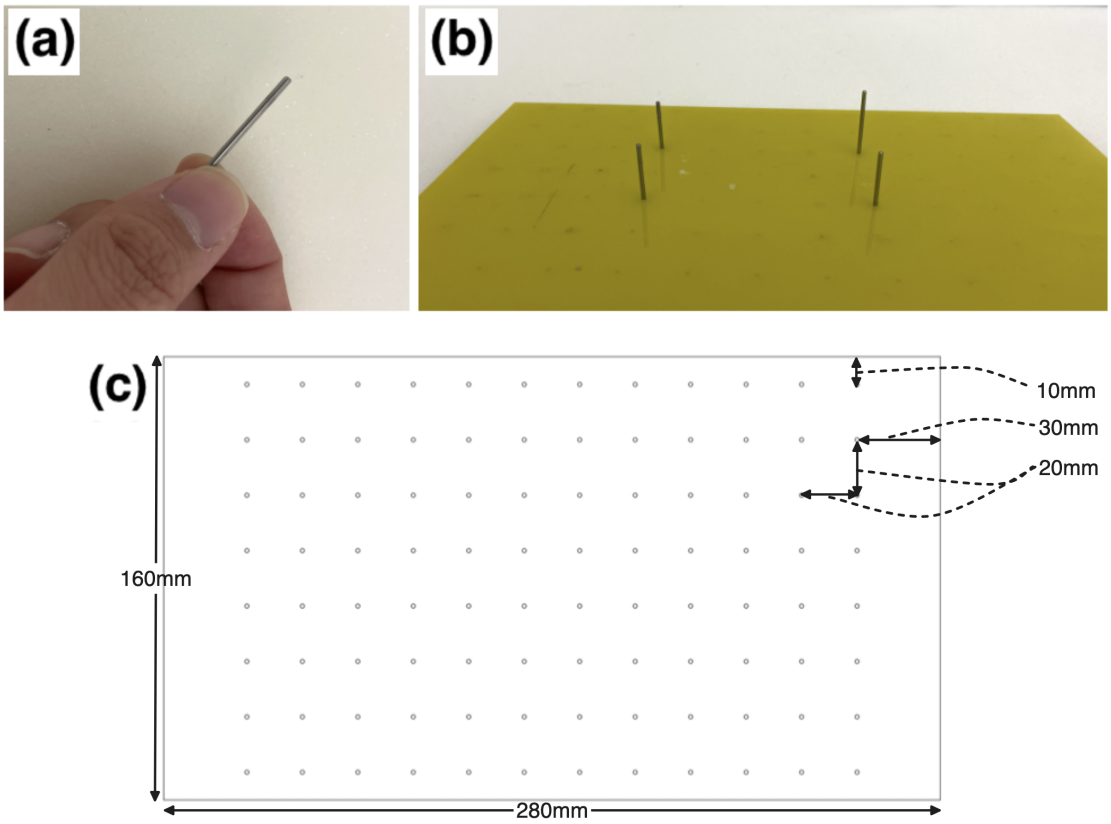

Figure 2.2: Materials required for lamination preparation: (a) Dowel pin for lamination. (b) Dowel pins inserted through the acrylic board. (c) Top view of the acrylic board with measurements and hole placement.

the laser cutter, tape all four sides of the sheet on the laser cutter base, and cut out the shape in Figure 2.3 c. Finally, carefully remove the cutout parts and leave the rest of the sheet (without the cutouts) in the laser cutter. Do not change or close anything on the laser cutter software.

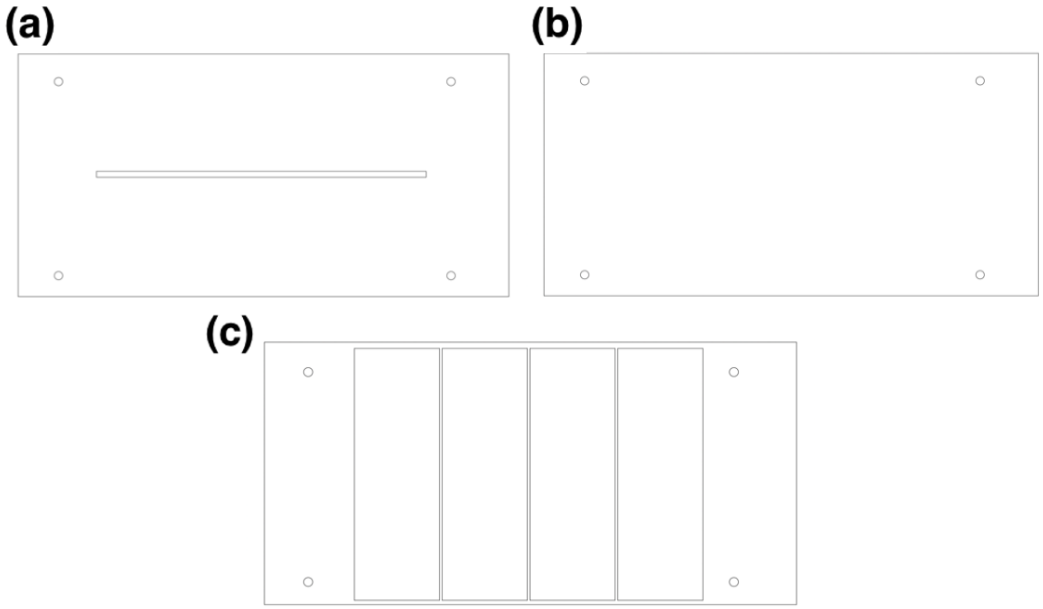

Figure 2.3: Laser cutting instructions for rigid, adhesive, and bioplastic material: (a) Top view of top and bottom rigid layer and adhesive layer cut drawing, with the open middle part to allow exposure of the bioplastic layer. (b) Top view of bioplastic thin sheet layer cut drawing. (c) Top view of the final cut, which produces four laminated pieces (see Figure 2.4). The four holes in each figure are used for dowel pin alignment (see Figure 2.2).

2.1.3 Step 3 Lamination

Place 4 rods apart on the acrylic board from the preparation step, same as the distances shown in Figure 2.3. Align the four circles on the bottom rigid material layer with the rods, then press them down onto the acrylic board. Next, use the same way to laminate one adhesive layer, with the sticky side facing down towards the bottom rigid material. Then, take out the whole piece (now with one adhesive layer on the bottom rigid layer), remove the non-adhesive paper of that layer, and carefully hold the side of the piece to align and place it back to the acrylic board.

Next, align and place the bioplastic layer the same way. Do the same for the other adhesive layer, and also remove the non-adhesive paper with the same technique as previously described. Last, place the top layer of the rigid material.

2.1.4 Step 4 Final Cut

Take the 5-layer laminated material out of the rods and acrylic board. Place the laminated piece on the hole cutout on the layers cut with the laser cutter in the previous steps. Ensure all four sides of the laminated piece are aligned with the hole on the leftover rigid material sheet. Then, cut the shape in Figure 2.3 c with the laser cutter using the same setting and location (note in the last step, the programming and position of the laser cutter were not and should not be changed).

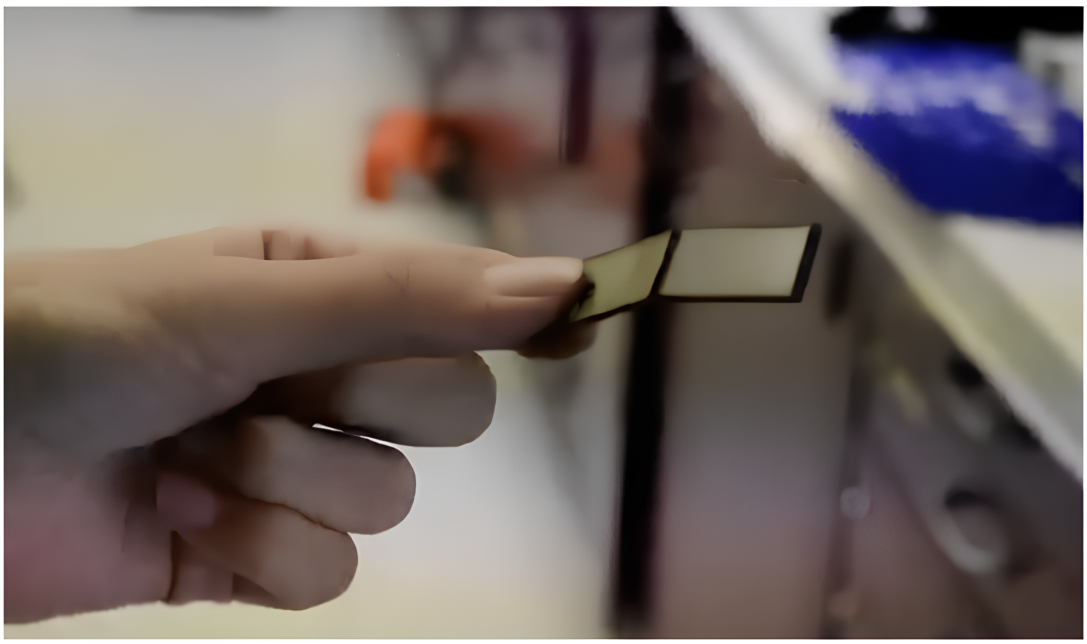

Figure 2.4: 5-layer laminated piece with the FR4 as the rigid layers and exposed bioplastic layer in the middle as flexure joint.

These steps allow us to obtain four individual pieces of the 5-layer lamination. An example of the resulting laminated piece is shown in Figure 2.4.

2.1.5 Lamination Exploration and Experimentation

Regarding material choices for the rigid layer (top and bottom outer layer in the 5-ply lamination process), two different materials were tested: cardboard and glass-reinforced epoxy laminate (FR4) (Figure 2.3 shows the laminate material with FR4 as the rigid layer).

Initially, cardboard was used for the rigid layer material as previous experiments in the lab have shown the cardboard's satisfactory response to adhesion. However, it was soon found that cardboard softens significantly as it absorbs water and is, therefore, not durable enough in high-humidity environments. Additionally, after absorbing water or moisture, cardboard has difficulties returning to its pre-wet shape even after thorough drying. These factors could cause significant reliability issues for the RHex robot when used in complex real-world environments and, therefore, ruled out cardboard as the rigid layer material.

To allow the Rhex robot to operate reliably in a wet environment, materials with low moisture absorption rates are needed. For this reason, FR4 was chosen. With a low moisture absorption rate of 0.10 % even when immersed in water for 24 hours [47], this should, in theory, allow FR4 to perform very well in humidity environments without durability or deformation issues that plague the cardboard material. It was also found (through experimentation) that the lamination process worked very well with FR4, with no obvious disadvantage over the adhesion strength of cardboard during lamination.

To see the difference between the dried and moistened pieces, force testing was conducted with the laminated piece in three conditions: dried, softened with two drops of water on one side, and softened with two drops of water on both sides. As shown in Figure 2.5, a servo motor was mounted on a steel rack, and the sample was attached to the servo motor's output shaft (with adapter). Then, a high-accuracy scale was placed under the sample. When the servo is rotated, the bottom half of the piece will strike on the scale and result in a weight reading (convertible to force) on the scale.

After several trials, it was found that the bending force required to bend the fully

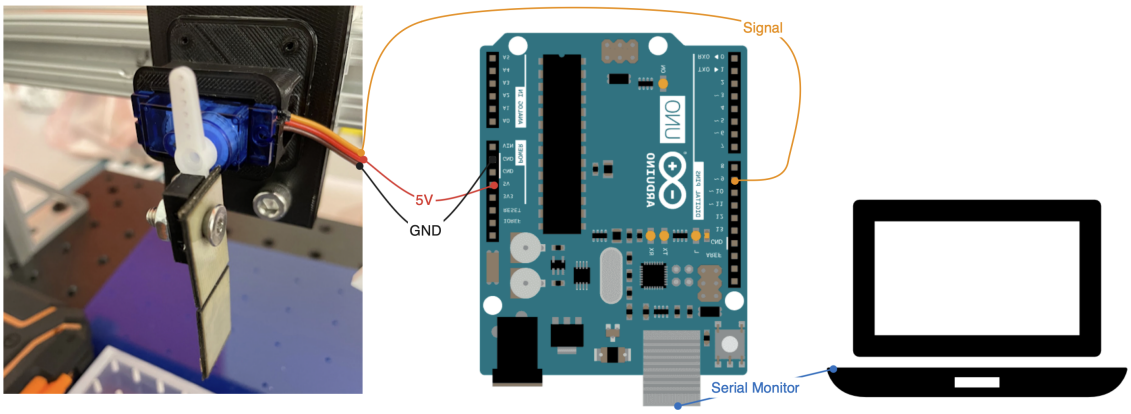

Figure 2.5: Wiring diagram for force testing setup. The setup is intended to test the bending force differences on the 5-layer laminated pieces in dried and moistened conditions.

dried bioplastic layers for about 75 degrees is generally between 0.02N and 0.03N, while only between 0.002N and 0.007N was required for the same bending angle if one side of the bioplastic is dripped with water. From this result, it is apparent that there is a significant difference in the material stiffness between dried and wet conditions.

However, after several trials, a crack was observed within the flexure joint (gap in the middle where the bioplastic was exposed) of the laminate material. The crack developed further with subsequent operations, and the laminate eventually broke into two pieces. The rest of the (unbroken) laminate pieces were also tested and exhibited similar flaws. Upon careful observation, it was found that the bioplastic sheet covered by the laminated top and bottom layers tends to be very dry, even when the middle flexure joint is exposed to water. It was speculated that this led the bioplastic in the flexure joint to be very soft while the surrounding material was very stiff, therefore fatiguing the flexure joint and ultimately leading to the crack and full failure. After multiple experiments and improvisations, it was ultimately concluded that the softened bioplastic sheet exposed in the middle could not handle the stress forces applied by the two laminated parts on each side.

From this experience, it was concluded that should it be possible to directly laminate the full sheet bioplastic on a supportive rigid layer, the full sheet may then be able to change its behavior with water while the inner rigid layer can still provide support.

Following this motion, plastic legs are 3D printed and laminated with a layer of bioplastic on top of it using the same adhesive layer. However, it was observed that the side of the bioplastic tends to wrinkle and rip off once it interacts with water or when exerted with a small force. Gummy glue was tested as an alternative adhesive in an attempt to remediate the issue, yet it was found to be unable to stick to the legs completely.

From these experiments and observations, it was ultimately decided that the sheet material is perhaps not the best option to be used on the legs of a RHex robot. We thus continued to investigate other options for utilizing bioplastic's variable rigidity.

2.2 Fabrication Technique: Molding

Learning from the previous issues with sheet bioplastic breaking, investigations have been carried out to find methods to make the bioplastic material more "rubbery" (with properties more similar to tires) with the hope that it would be more durable, flexible, and less prone to cracking and breaking. To achieve these goals, we iterated in parallel on both finding a better manufacturing process (i.e. molding, section 2.2.1 and section 2.2.2) and a more durable composition (formula in Table 2.1, section 2.2.3) for the bioplastic material.

2.2.1 Mold Designs Iteration

Initially, the process of making bioplastic involves pouring the formulated bioplastic solution (liquid) into a curing pan and waiting until it's fully dried [32]. During the drying process, the bioplastic solution is spread evenly (by gravity) into a shallow layer on the bottom of the flat curing pan and would, therefore, result in a very thin sheet of solid bioplastic once dried.

In order to make the bioplastic more flexible (and "rubbery-like"), the bioplastic layer will have to be thicker. Considering that the curing pan may not be able to dry the thick layer of bioplastic thoroughly and evenly, a curing mold would be needed to shape and cure the bioplastic into shapes desired for the RHex legs.

There is a total of three iterations for the curing mode. The first two versions are unsuccessful prototypes, and only the third (and last) version is used in final

production.

The first iteration of the curing mold is shown in Figure 2.6. It consists of two parts: a hollow C-shaped body and a flat bottom panel. The mold was made with an Ultimaker 3D printer and polylactide (PLA), and taped together over all the seams to ensure water-tightness. The bioplastic solution was then poured inside and left to cure.

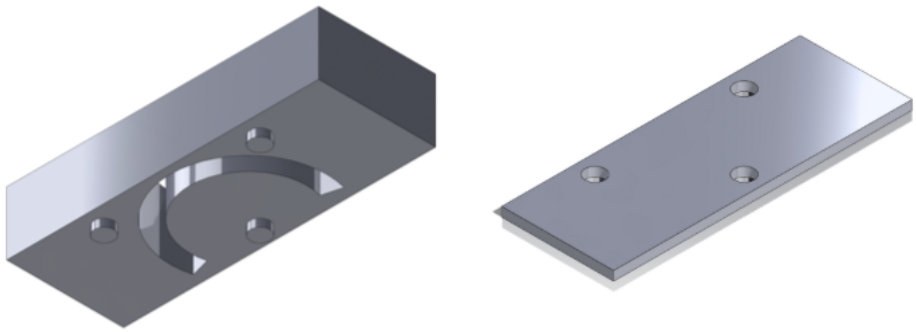

Figure 2.6: Isometric view of the first version of the mold used to cure bioplastic. The mold consists of two parts: a hollow C-shaped body (left) and a flat bottom panel (right). Both are made with an Ultimaker 3D printer and then assembled and taped to ensure water-tightness. Bioplastic solution is then poured into the vacant space on the top mold.

However, it was soon discovered that despite the bioplastic being able to cure correctly into a uniform solid structure with the mold, it remained extremely soft and could not support the weight that would be reasonable for a small robot, nor would it respond to humidity changes in any significant way due to its inherent softness. Spencer, a member of the lab specializing in materials science, suggested that a gelatin solution, a simpler alternative, would exhibit similar post-curing properties, and it would be possible to then attach or laminate a thin layer of bioplastic onto the outer side of the gelatin post-curing.

To investigate the possibility of this suggestion, a leg was constructed using a gelatin solution without genipin (omitting crosslinking), which, akin to the prior iteration, displayed minimal reactivity to water. Proceeding to enhance the leg's properties, we undertook the lamination of a bioplastic sheet onto the side of the C-shaped gelatin leg without crosslinking, assuming that the lamination process would

be simple due to the materials having similar compositions. However, the results were similar to previous experiments, where the bioplastic sheet easily detached from the gelatin trunk even after extensive adhesive application (see 2.1.5). Subsequently, an alternative method to enhance adhesion using both surface heat and humidity was explored in hopes that heat would induce stickiness and help with the lamination process. To achieve this, the gelatin leg was left in a 45°C oven for 10 seconds (extended exposure risked liquefaction), followed by pressing the bioplastic sheet onto its surface, placing it in a mold, and then refrigerating. However, limited success was achieved with these attempts, as the sheet bioplastic still failed to adhere securely and would delaminate even when subjected to minimal force.

To overcome the difficulty in adhesion, a different approach was devised, where the sheet bioplastic would be directly cured with the fresh gelatin solution. This should, in theory, allow the bioplastic sheet to crosslink and bind with gelatin during the curing process and, therefore, forego the need for adhesion and lamination. To achieve this, the bioplastic sheet was positioned alongside the mold, and a fresh gelatin solution was prepared and poured into the mold while the bioplastic sheet was in place. Unfortunately, as soon as the gelatin solution is poured in, the sheet material loses its stability and develops wrinkles once on its surface, presumably caused by a combination of the heat from the gelatin solution and the ambient humidity. Despite extending the waiting time after the gelatin solution reaches 45°C to the maximum possible (would risk permanent curing if waited any further), the issue persists.

In response to these challenges, a new approach was explored where mechanical methods were used to fasten the bioplastic sheet and gelatin together. To achieve this, bulb-shaped mounting points were designed onto the surface of the gelatin leg, intended to be fastened to the bioplastic sheet by piercing the sheet itself. The bioplastic sheet will be cut to exhibit "x" shaped cuts on the mating points with the gelatin bulbs and be popped over the bulbs such that it will be mechanically held to the gelatin leg's outer surface.

A second version of the mold was designed for this purpose, as depicted in Figure 2.7 a-c.

However, upon removing the legs from the mold, the bulbs on the gelatin leg were found to be extremely fragile, necessitating delicate removal with a Q-tip and precision blade. Additionally, attempts to insert the sheet bioplastic often resulted in

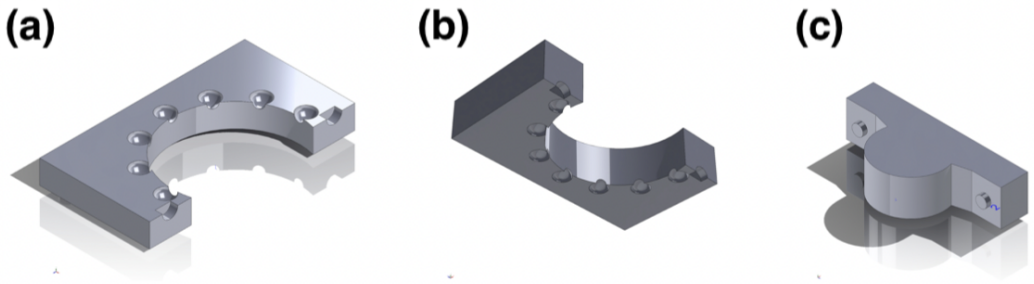

Figure 2.7: Isometric view of the second version of the mold used to cure bioplastic. (a) Bottom half of the bulb side. (b) Top half of the bulb side. (c) Third part to hold the mold pieces together. All pieces are made with an Ultimaker 3D printer and then assembled and taped to ensure water-tightness. Bioplastic solution is then poured into the vacant space on the top mold.

the breakage of these fragile bulbs. Even with several modifications to the mold, it has only managed to achieve a 70% success rate. Also, the composite leg is still extremely vulnerable to breakage when subjected to minor force, and the gelatin material in the leg is very susceptible to deterioration if not stored at a cool temperature.

After multiple failures, we revisited a previous experiment involving a thick bioplastic leg with crosslinking crafted several days prior. We noted that this leg exhibited increased hardness compared to the hardness several days ago. Unlike the sheet material, which dried at the culmination of its curing process, the thick bioplastic's curing concluded in a wet state, requiring additional days to dry completely after extraction from the mold. We attempted to spray water on the dried, thick bioplastic leg, and were pleasantly surprised to observe a softening effect.

This discovery led us to fall back to the previous approach of directly molding bioplastic into thick legs and thus abandoning the use of bioplastic sheets and lamination/mechanical fastening approaches.

2.2.2 Final Mold and Mold Preparation

With the re-introduction of the original bioplastic manufacturing process, several changes were made to improve the effectiveness of the mold. Notably, five changes were made based on the first and second iterations.

Firstly, it was noticed that in the previous iterations, the top of the bioplastic

liquid around the fill hole lost water more rapidly than the rest of the liquid deeper in the mold. This has led to frequent distortions in the end product. Thus, a top panel was added (see Figure 2.8) to cover the fill hole. Secondly, more structural support was added such that the different structural pieces comprising the mold would fit more tightly together. This allows the mold to be more air-tight and water-tight and avoids bioplastic solution leaking slowly from the seams of the mold, as exhibited in the previous iteration of the mold. Thirdly, Form 3 3D printers are utilized to print the mold for higher precision (as compared to previous usage of Ultimaker printers). This allows the inner surfaces of the mold to be smoother and, therefore, allows the dried bioplastic leg to have smooth surfaces.

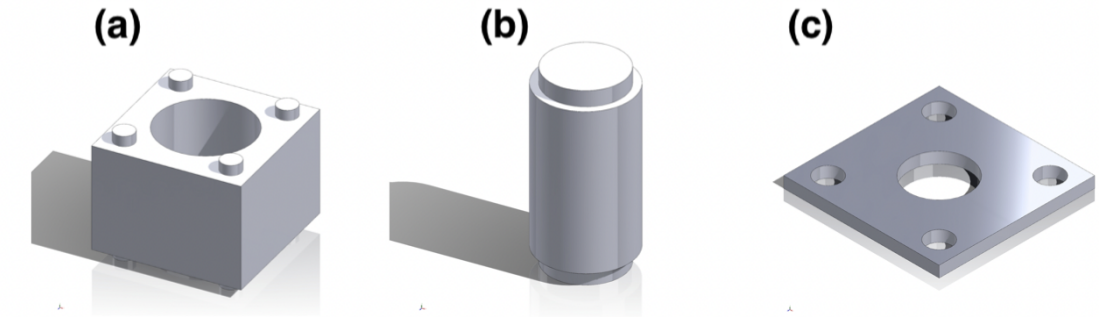

Figure 2.8: Isometric view of the final version of the mold used to cure bioplastic. The mold consists of three parts: (a) Mold body. (b) Inner cylinder. (c) Cover for top and bottom (total of two to cover both sides). All pieces are printed with a Form 3 3D printer. Part (a), (b), and one piece of (c) are assembled first. Bioplastic solution is poured into the vacant space from the top. The other piece of part (c) is then assembled on top to secure parts (a) and (b).

Additionally, different resin materials were also tested for mold printing to determine if a particular type of resin would lead to better performance in the final mold regarding bioplastic surface smoothness and ease of separation. Specifically, both white photopolymer resin (RS-F2-GPWH-04) and clear photopolymer resin (RS-F2-GPCL-04) are tested. It was observed that even after sanding the surface of both molds, the mold printed with clear resin still had small dots on the inside of the mold, while the molds printed with white resin did not exhibit the issue. Therefore, white photopolymer resin (RS-F2-GPWH-04) was chosen as the final mold material.

Finally, different printing techniques are used to increase mold surface smoothness

and further decrease the need for sanding. When utilizing the software for mold slicing, it is crucial to tilt the components and generate appropriate support, as tilting enhances the precision of the final product according to Form 3 printing's official guidelines. When creating supports, special attention should be given to minimizing or omitting support on the inner surface of Figure 2.8 a, the outer surface of Figure 2.8 b, and one of the larger sides of Figure 2.8 c. If excessive support is generated in these regions, it is necessary to re-tilt the part and regenerate support. This is extremely important to the final performance of the mold as these areas come into direct contact with the bioplastic solution during the casting and curing process. Since breaking the support after printing often leaves a small residue even after careful sanding, it may result in unwanted dents or unevenness in the final bioplastic product. Therefore, proper tilting and support generation are essential in this phase to mitigate defects in the final bioplastic casting and to reduce the need for extensive sanding.

2.2.3 Material Composition Iteration

The initial composition starts with the original bioplastic sheet formula. The water gelatin ratio in this formula is 85:15 and contains 48% glycerol [32].

After repeated testing, Modifications were made to increase the dried stiffness and decrease the wet (or humidified) stiffness. In order to increase the dried stiffness, the water-gelatin ratio was increased to 80:20 (more gelatin in the same amount of water). This is likely already the minimum water-gelatin ratio possible, as this is reaching the limit of the amount of gelatin that can be dissolved in the solution. To further enhance durability and prevent the thick bioplastic leg from cracking, the glycerol percentage (relative to gelatin mass) was increased to 75%. Finally, to retain stiffness with these modifications to the formula, the gelatin needs to bloom longer at room temperature (see configuration and steps below).

The final mold (see section 2.2.2) requires a total of 60ml of bioplastic solution to fully fill. The amount required for each individual ingredient is listed in Table 2.1 below.

It is recommended to make the solution in 3 separate sets of beakers and vials to eliminate the possibility of the gelatin not being able to dissolve in water within the

time frame specified and also to minimize spillage during the stirring process. Note that the solution needs to be made together in one batch, as otherwise, when the solution is poured into the mold, it would start curing and, therefore, be unable to combine smoothly with any additional solution subsequently.

The specific steps are listed below:

1. Put DI water 1 in a graduated cylinder.
2. Mix gelatin, DI water 1, and glycerol ingredients together in a beaker. Wait for 45 minutes so that the mixture can hydrate.
3. Cover the beaker with a plastic wrap, then heat the beaker in the oven at 60°C for an hour.
4. While waiting, prepare genipin.
5. Add ethanol, DI water 2, and genipin to a glass vial. Genipin should be stored in the freezer. Make sure to put it back after using it.
6. Gently swirl the vial to dissolve the mixture. A light yellow genipin solution should appear.
7. Take the gelatin mixture out of the oven and put it on a 55°C hot plate. Stir with a stir bar at 300 rpm (the stir bar must be fully submerged)
8. Put a thermometer in the mixture, and when the gelatin mixture has reached around 55°C, slowly add the genipin solution.
9. Keep stirring the mixture for about three minutes. The mixture should now be smooth and blended.

Bioplastic formula for a total amount of 20.5ml:

Deionized (DI) Water 1:	14.287g	Ethanol:	1.5g
Gelatin:	3.572g	Deionized (DI) Water 2:	0.75g
Glycerol:	2678.6mg	Genipin:	145mg

Table 2.1: Formula for making the bioplastic legs

10. Take the mixture out of the hot plate. If bubbles are present in the mixture, add several drops of ethanol to remove them.
11. Remove the stir bar and follow the steps in the next section (2.3) to make the bioplastic legs.
12. Clean up any glassware or materials used, turn off the hot plate, and ensure the genipin is returned to the freezer.

In addition to the percentage and ratio adjustments, cellulose 'reinforcement' was also tested during the formulation process. However, no significant change or advantages in either material properties or stiffness change were observed from adding the cellulose fibers. The steps for making gelatin-cellulose formulation (13% cellulose) are listed below in case of future research interest:

1. Put DI water 1 in a graduated cylinder.
2. Mix gelatin, DI water 1, and glycerol ingredients together in a beaker. Wait for 45 minutes so that the mixture can hydrate.
3. Cover the beaker with a plastic wrap, then heat the beaker in the oven at 60°C for an hour.
4. While waiting, prepare genipin.
5. Add ethanol, DI water 2, and genipin to a glass vial. Genipin should be stored in the freezer. Make sure to put it back after using it.
6. Gently swirl the vial to dissolve the mixture. A light yellow genipin solution should appear.
7. Take the gelatin mixture out of the oven and put it on a 55°C hot plate. Stir with a stir bar at 300 rpm (Note: the stir bar must be fully submerged to prevent incorporation of air; use a smaller beaker as needed)
8. Once the gelatin mixture has reached 50-55°C (use thermometer), slowly add the desired cellulose % based on your gelatin content (e.g. 13% = 3.572g * 0.13)
9. Perform the same process for adding the genipin solution.
10. Allow the mixture to stir for about three minutes. The mixture should become smooth and homogeneous. If bubbles are present in the mixture, add several drops of ethanol to remove them.

11. Remove the stir bar and follow the steps in the next section (2.3) to make the bioplastic legs.
12. Clean up any glassware or materials used, turn off the hot plate, and ensure the genipin is returned to the freezer.

2.3 Making the Bioplastic Legs

After obtaining the accurately printed mold (see section 2.2.2) and the correct formula (see section 2.2.3), it is possible to make the bioplastic legs.

Started the molding process by spraying the mold release spray on the internals of the mold evenly. Place the mold in an air scrubber chamber for at least 10 minutes to allow the mold release spray to form a film on the mold surfaces that contact the bioplastic. This allows for a higher success rate when releasing the bioplastic from the mold after curing.

Then, assemble the bottom section mold while leaving the top cover absent. To prevent potential leakage, flip the assembled mold vertically (with the bottom facing up) and use masking tape to securely cover the bottom and side seams of the mold separately to ensure water-tightness. Perform the same taping procedure with duct tape or electrical tape to hold the masking tape in place.

Pour the previously configured solution into the mold from the absent space at the top of the body section, and secure the top cover onto the mold with the smooth side facing down. Use masking and duct/electrical tape as required to secure the top cover.

At this state, leave mold upright in a dry and ventilated area and wait at least 36 hours for the bioplastic liquid to cure.

After the curing process is completed, peel off the protection tape and remove the top and bottom covers of the mold. Carefully use an X-acto blade to remove any bioplastic film around the seams of the mold, and then gently and slowly push the middle cylinder from bottom to top while ensuring the cylinder is not slanted during the push. The bioplastic casting should come out of the mold with the middle cylinder mold. In case it does not come out with the cylinder (may happen if the mold release is not sprayed enough), it is usually possible to use a clean Q-tip to push

it out gently. Take out the center mold cylinder and expose the hollow bioplastic cylinder.

Inspect the inner and outer surfaces of the bioplastic hollow cylinder and make sure they are generally smooth. If excess dots and dents are observed (likely due to bubbles in the solution), discard the bioplastic cylinder and repeat the molding process with additional ethanol in Step 10 of section 2.2.3.

Reinsert the center mold cylinder and leave the bioplastic casting in a cool and ventilated room for at least four days to fully dried.

Once the bioplastic hollow cylinder is fully dried, take out the center cylinder mold. In order to make bioplastic legs, the hollow cylinder has to be cut into smaller pieces by a bandsaw.

Firstly, the top and bottom of the cylinder are cut by 5 mm to ensure uniform thickness over the remaining cylinder. This is because the top and bottom ends of the dried cylinder are always slightly thicker than the middle part due to the molding process. Secondly, an extra middle cylinder mold is printed using an Ultimaker 3D printer with PLA (infill density of 15% and infill height of 0.15mm). It is inserted into the hollow part in the middle of the bioplastic cylinder. This provides structural support for the bioplastic cylinder so that it does not deform during the cutting process and cause the cut surface to be misaligned. The bioplastic cylinder (with the PLA insert) is then cut with a bandsaw into the shape of legs, as depicted in 2.9. Finally, collect the legs and wipe clean with towel.

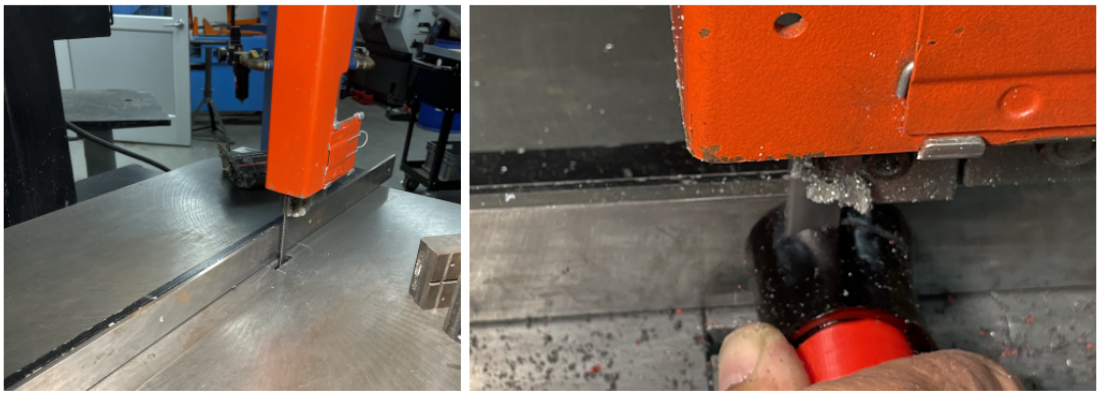

Figure 2.9: The cutting setup with bandsaw (left) to cut the cured bioplastic piece into legs usable for the robot, and close-up view (right) for cutting the bioplastic legs when placed on the PLA middle cylinder support so that the legs could maintain its shape and be cut easily.

Chapter 3

Characteristic Analysis and Hardware

3.1 Characterization Experiment

The part that enables the robot to change in locomotion with respect to different humidity environments is the bioplastic legs. The tunable stiffness of bioplastic legs allows the robot to have softer legs in high humidity and stiffer legs in low humidity. This chapter details the characterization experiments conducted on the legs, including a material repeatability test to understand the repeatability of the experiments with the legs and a force-displacement test to understand how the bioplastic legs respond to different durations of exposure to environmental humidity levels.

3.1.1 Repeatability Test

This repeatability test was conducted to ensure that all of the following experiments detailed in this chapter and Chapter 4 are repeatable. This test aims to show that the bioplastic legs are able to return to their original state after being subjected to external forces by the force sensor, and that the force reading for each push should be similar such that the characteristics of the bioplastic material do not change permanently after the exerted force is removed. The setup and process are shown in Figure 3.1. In the setup, a Transducer Technology GSO-500g load cell (+/- 0.0025

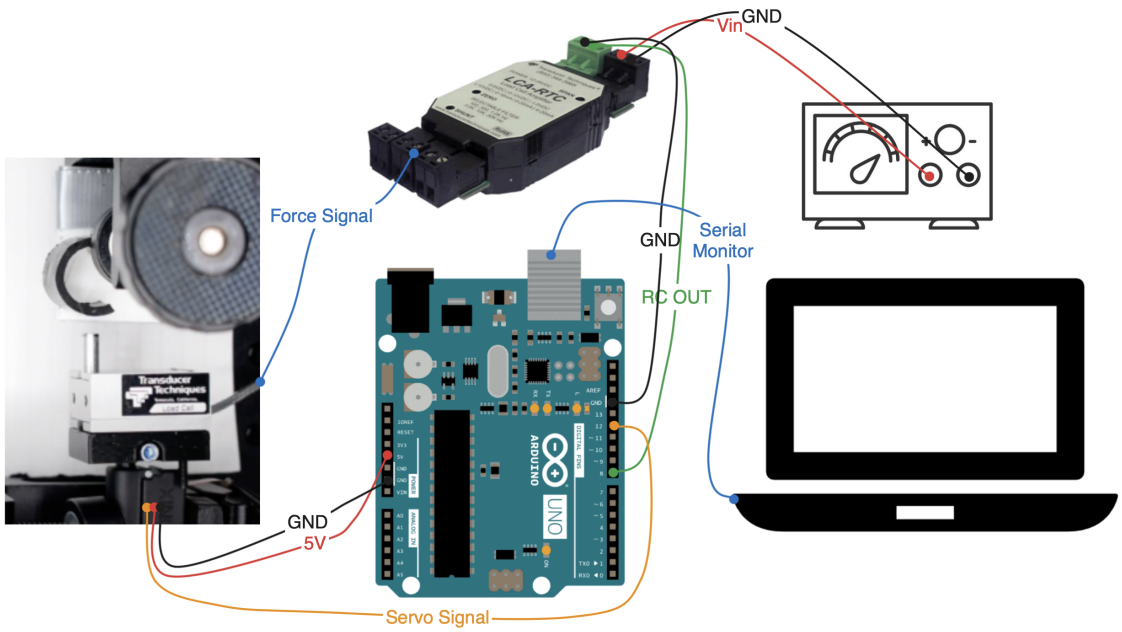

Figure 3.1: Wiring diagram for repeatability testing the bioplastic leg. Both load cell and linear actuator are attached to Arduino for reading and control. Data is collected from Arduino's serial ports to a computer and then analyzed.

N, see Appendix B.2 for specifications) is attached to an Actuonix linear actuator L16-35-50 (+/- 0.3mm, see Appendix B.1 for specifications), and an LCA-RTC load cell amplifier is used along with an Arduino UNO to read the values to the laptop. The pushing location was marked on the leg and aligned with the load cell trigger such that the load cell would push onto the exact same location on the bioplastic leg each time. The tests were conducted when the bioplastic leg was 0 minutes (fully dried), 15 minutes, 30 minutes, and 60 minutes in the humidity chamber that was set to 75% relative humidity (RH) and temperature of 25°C. The bioplastic leg was pushed 5 mm for a total of 25 times (5 trials, with each trial consisting of 5 pushes) in each humidity setting. An example of the repeatability testing results (one trial of pushing the fully dried leg, after being converted from sensor raw data into force data) is shown in Figure 3.2.

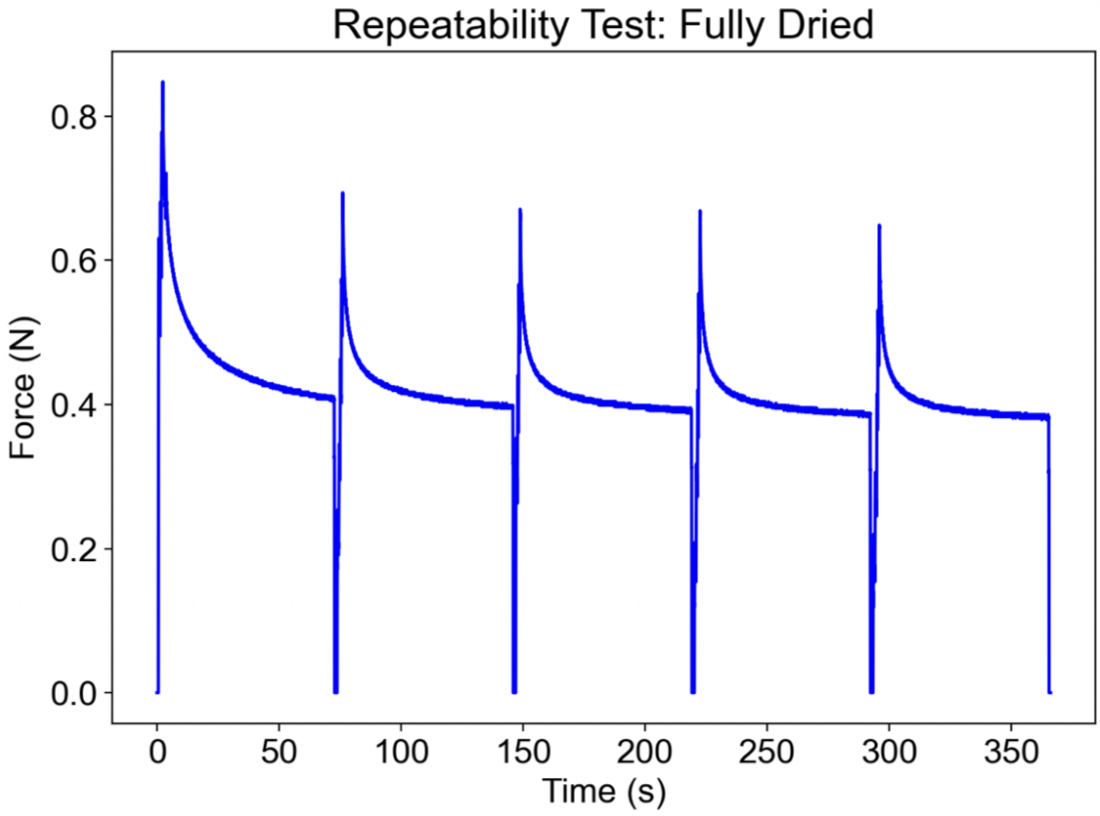

Figure 3.2: Repeatability test result plot example (one trial) for fully dried bioplastic leg, after being converted from raw data to force data.

Note that the unit of the sensor's output data is in raw data format. To find the corresponding force data, the conversion formula between Force (N) and the raw data format was constructed after repeated calibrations to the load cell:

$$Force(N) = Data_{raw} * 50 * 0.0098/126$$

To find the standard deviation, the raw data was converted to newtons, and the values of the stabilized state (when the difference between the maximum and minimum for every ten consecutive values is less than 2%) were taken to ensure the readings measure the force required to compress the bioplastic material exactly 5 mm stably. The standard deviation of each respective test was computed using the stabilized state values. See Table 3.1 below for force reading standard deviations corresponding to each dryness of the bioplastic material.

Time in humidity chamber	Average Force Reading	Standard Deviation
0 minutes (fully dried)	0.417N	0.01314
15 minutes	0.323N	0.00950
30 minutes	0.282N	0.00657
60 minutes	0.249N	0.00626

Table 3.1: Average force reading and standard deviation calculated from the repeatability test for bioplastic legs in different humidity levels. Note that the standard deviation is low, meaning that the legs respond to forces very similarly during repeated exertions, and do not permanently deform or result in characteristic changes after the exerted force is removed. Note also that the average force readings decrease as the duration of exposure in the humidity chamber increases. This means there is a stiffness change in the bioplastic leg in different humidity environments.

Observe from the table that the standard deviation is low, showing that the legs respond to forces very similarly during repeated force exertions and do not permanently deform or result in characteristic changes after the exerted force is removed. Observe also that the average force readings decrease as the duration

of exposure in the humidity chamber increases. This shows that stiffness changes occurred in the bioplastic leg as a result of different durations of humidity exposure.

In conclusion, we find from the repeatability testing that the bioplastic material is able to return to its original state and material characteristics after being decompressed 5 mm by an ephemeral force. We also find that the force required for decompression is significantly lower after exposure to humidity.

3.1.2 Force-Displacement Test

After ensuring that experiments were repeatable, a force-displacement test was also conducted using a similar setup to find the spring constant of the bioplastic material. Instead of being pushed for 5 mm with the force sensor and retracting completely, the bioplastic leg was pushed for 1.6 mm each time for a total of 4 continuous pushes. Readings were taken at each pause after the force readings stabilized (when the difference between the maximum and minimum for every ten consecutive values is less than 2%) to ensure the readings measure the force required to compress the bioplastic material exactly the amount required. This setup provides five force readings (at 0 mm, 1.6 mm, 3.2 mm, 4.8 mm, 6.4 mm) for each trial. The trial was repeated five times for the bioplastic legs, thus yielding a total of 25 readings. The test was conducted with bioplastic legs that were exposed for 0 minutes (fully dried), 15 minutes, 30 minutes, and 60 minutes in the humidity chamber that was set to 75% relative humidity (RH) and 25°C. An example of the force-displacement testing results (fully dried) is shown in Figure 3.3.

Note that the unit of the sensor's output data is in raw data format. To find the corresponding force data, the conversion formula between Force (N) and the raw data format was constructed after repeated calibrations to the load cell (see also section 3.1.1):

$$Force(N) = Data_{raw} * 50 * 0.0098/126$$

After converting to newtons, it is possible to plot the force-displacement curve of each humidity by using readings from the force sensor (see fully dried test result example in Figure 3.3). The plotted force-displacement curves for 0 minutes (fully dried), 15 minutes, 30 minutes, and 60 minutes of exposure in a humidity chamber are shown in Figure 3.4 below.

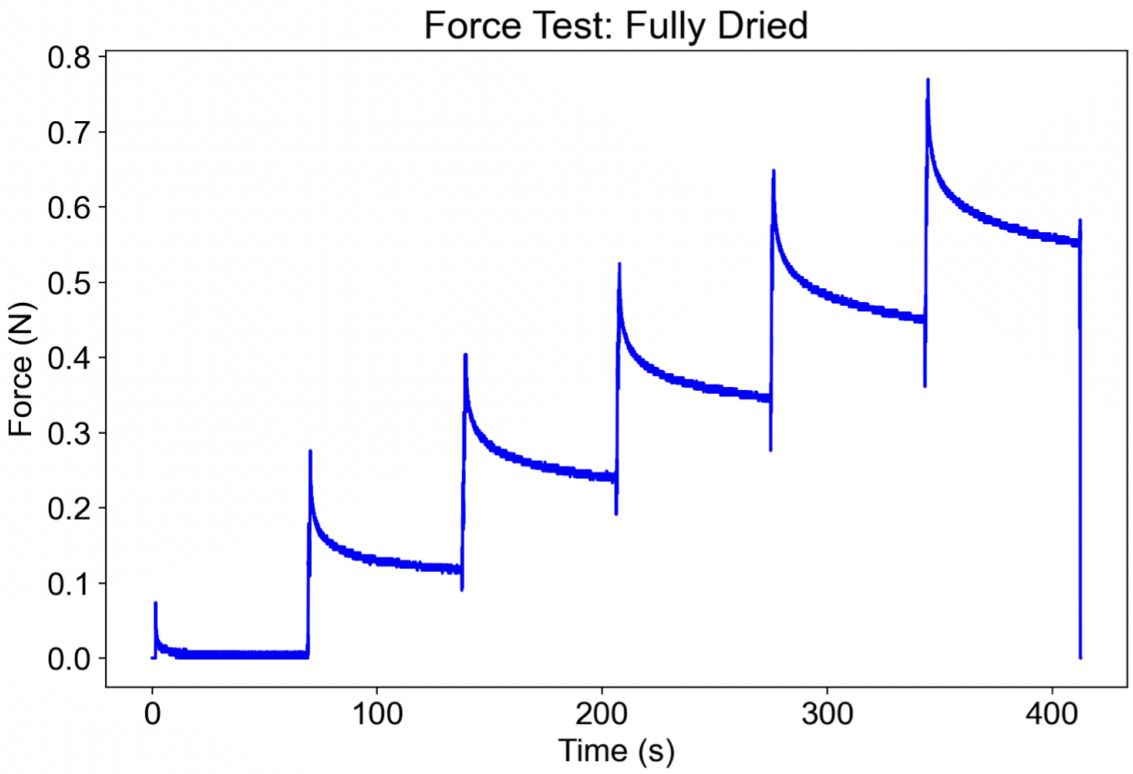

Figure 3.3: Force test result plot (one trial) for fully dried bioplastic leg after being converted from raw sensor readings to newtons. The 6 stabilized reading (plateaus in force readings in graph) corresponds to: actuator fully retracted, aligned and barely touching the leg (0 mm), pushed 1.6 mm, pushed 3.2 mm, pushed 4.8 mm, and pushed 6.4 mm

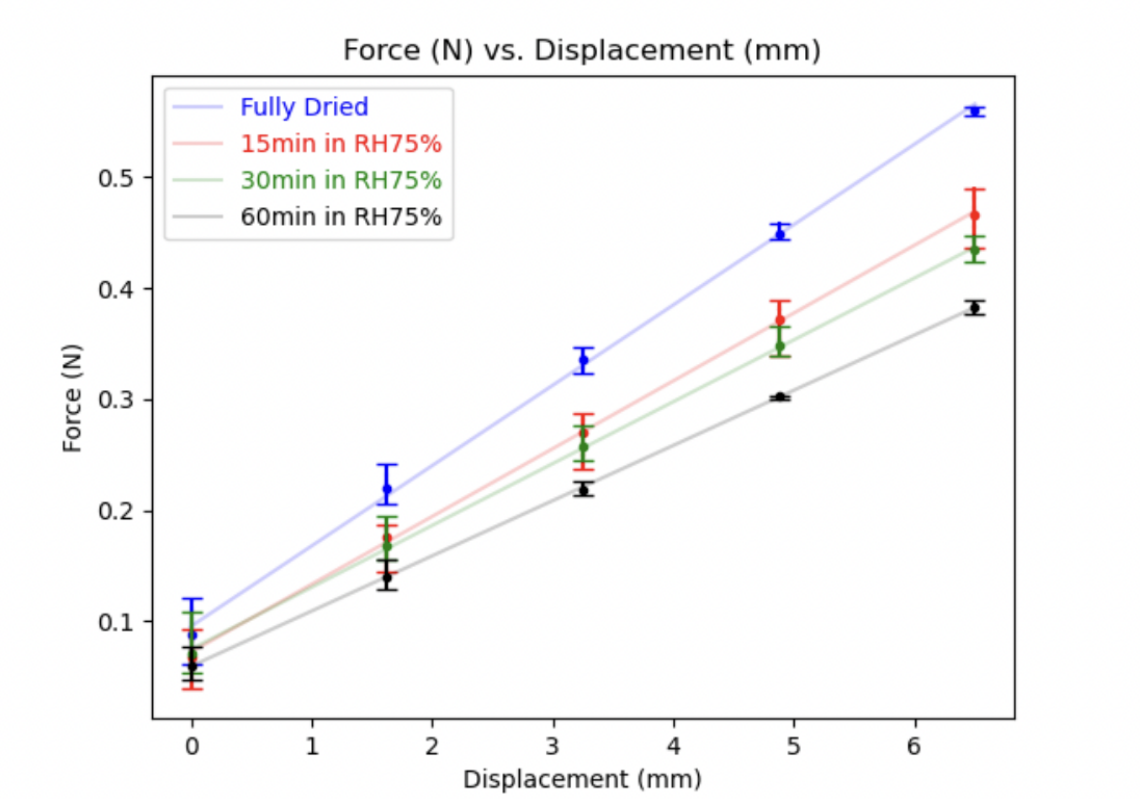

Figure 3.4: Force displacement diagram for bioplastic legs with color-coded humidity conditions. The slope of each force-displacement line is used to find the spring constant of the bioplastic leg in each humidity.

Proceed to calculate the spring constants of bioplastic leg with various humidity exposures by computing the slope of each trend line in the force-displacement diagram 3.4, as in Table 3.2.

Time in humidity chamber (minutes)	Spring Constant (N/mm)
0 minutes (fully dried)	0.072 N/mm
15 minutes	0.061 N/mm
30 minutes	0.056 N/mm
60 minutes	0.05 N/mm

Table 3.2: Spring constants calculated from the force displacement diagram (Figure 3.4) for bioplastic legs with color coded humidity conditions

Observe from the table of spring constants that as exposure in the humidity chamber increases, the spring constant of the bioplastic legs decreases accordingly. This shows that environmental humidity is affecting the stiffness of the bioplastic leg inversely paired with exposure duration (i.e. longer exposure leads to less stiff legs).

3.2 Robot Iteration

To explore the performance of bioplastic on robots in real-world scenarios, a suitable robot must be chosen to be compatible with bioplastic legs and benefit from humidity-based stiffness tuning. This section details the robots developed to fulfill this purpose, along with their advantages and limitations.

3.2.1 TinyRhex

To test the bioplastic legs, a lightweight RHex robot (TinyRhex) was designed.

The TinyRhex was designed such that it can hold six continuous servo motors, with one bioplastic leg attached to each servo motor (Figure 3.5). To ensure the efficiency and cost-effectiveness of the robot, we drew inspiration from the CMU course 16-235 "Fantastic Robots and How to Fold Them", and employed the origami folding

technique to construct the shell of the robot. Thin polyethylene terephthalate (PET) was selected for the shell, considering its strength and water-resistant properties.

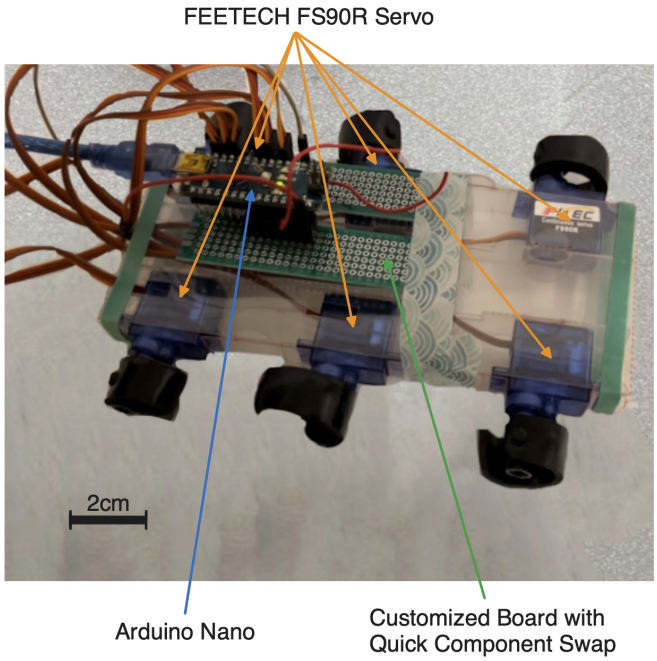

Figure 3.5: TinyRHex with PET folded robot body, six continuous servo motors, and bioplastic legs attached to each servo motor. Note the modular circuit design utilizing hot-swappable sockets for servo and Arduino connection.

To construct the shell of TinyRhex, a thin layer of PET (0.5 mm thick) was laser cut according to the cut file shown in Figure 3.6. In the figure, the left half is the top of the robot shell, and the right half is the bottom part. Note that the solid lines are intended to be cut through, while the dotted lines indicate the axes to fold the sheet into TinyRhex's shell.

During the cutting process, the PET sheet was unrolled and taped onto an acrylic board to prevent unintentional movement or vibrations. The Z value on the laser cutting software was set to 0.6 mm (slightly larger than the thickness of the PET sheet) so that the PET sheet would be cut through while the acrylic board underneath would remain reusable. The stroke value used for the cut file was 0.001 pt. After cutting, the sheet is bent along the dotted lines and folded into the TinyRhex shell along with FS90R continuous servo motors (Figure 3.7). If the shell does not hold its

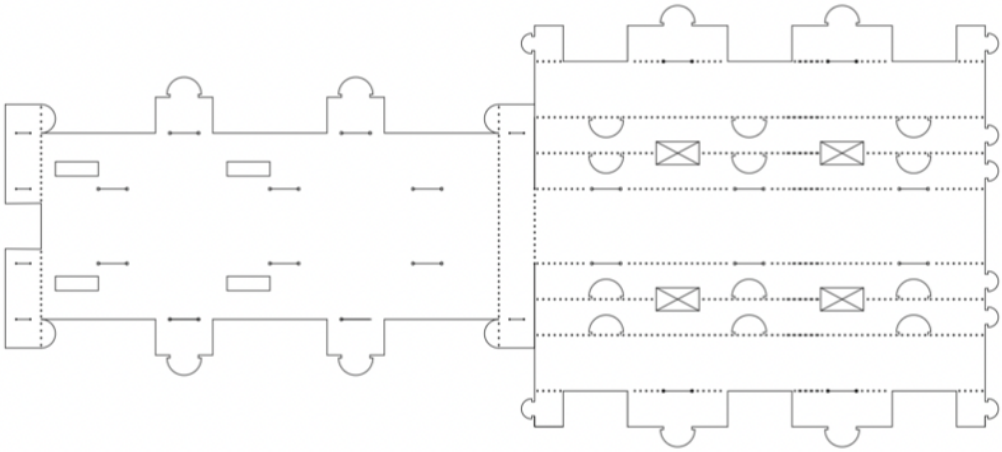

Figure 3.6: Top view of the Tiny RHex cut file. The shape depicted is laser cut onto clear PET and folded into the TinyRHex robot following the dotted lines in the photo. The folding process is depicted in Figure 3.7

position after bending, the laser power and stroke size should be increased. Inversely, if the shell breaks during bending, the laser power and stroke size should be decreased.

An Arduino Nano is attached to the top of the robot to control the servo motors. A modular circuit design utilizing hot-swappable sockets was implemented to allow the servo motors and Arduino to be easily maintained or replaced without requiring soldering and desoldering. The circuit is soldered onto two prototype boards (see Figure 3.8 for front/back wiring diagrams), and a 9V battery is attached to the Vin and GND ports of the Arduino to provide power to the controller. The six servo motors are then attached to the six PWM pins on the Arduino Nano board (D3, D5, D6, D9, D10, and D11) for control signal and are powered by the Arduino's 5V and GND pins.

In order to attach the bioplastic legs to the servo motors, a micro servo motor adapter is connected to the motor's output shaft in order to serve as a mounting platform for the bioplastic legs. A hole is then drilled at both the center of the servo motor adapter and at one end of the bioplastic leg (center position with regard to width) with a size 44 drill bit. Note that the hole should pierce the entire servo motor

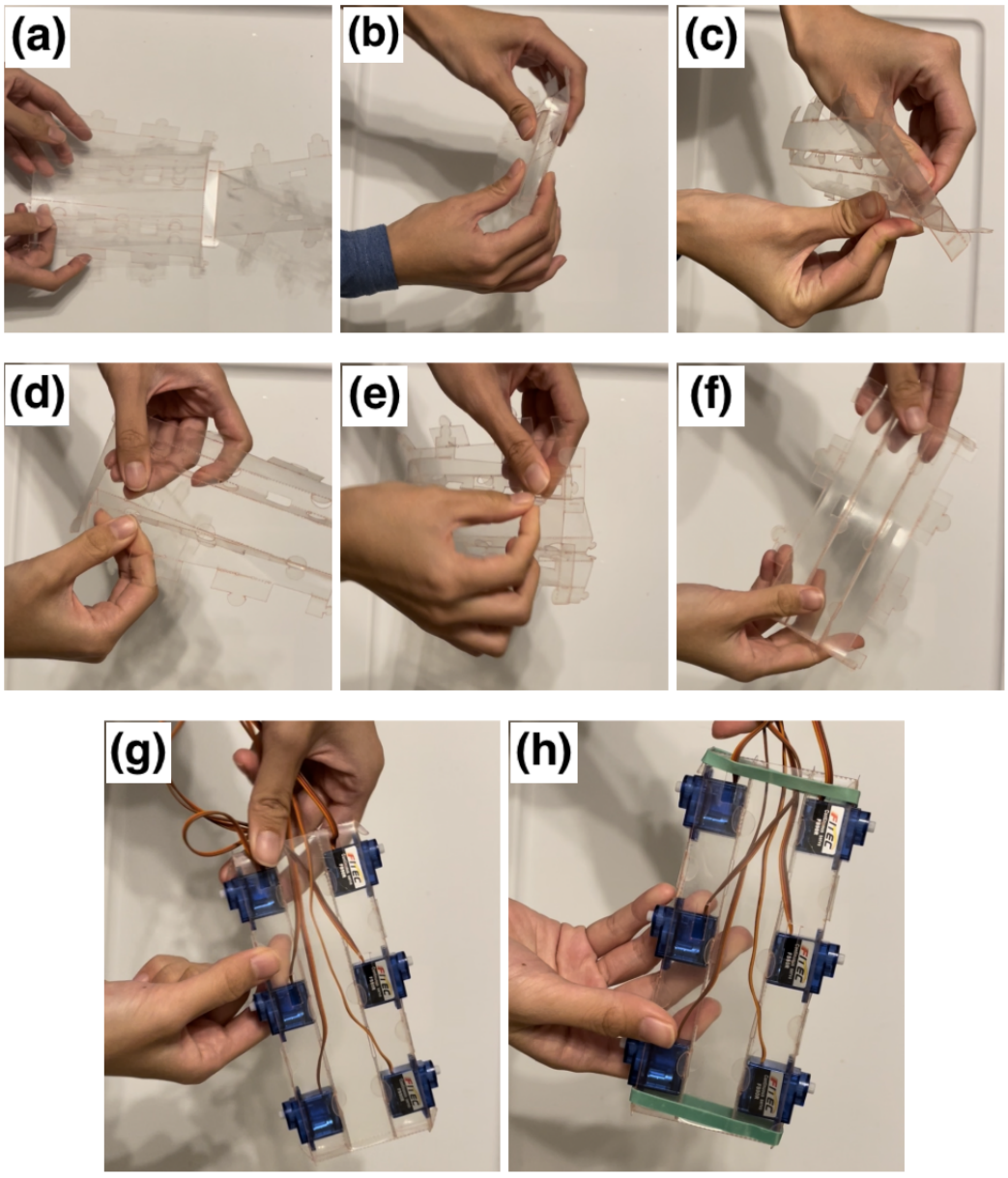

Figure 3.7: Process of folding TinyRHex: (a) Prepare the cut. (b) Bend the middle rectangle to form the top and bottom of the robot body. (c) Squeeze and fold the bottom to make slots for motors. (d) Secure the fold. (e) Pull the bottom cut from the top. (f) Middle of the body after previous steps. (g) Put the motors in and fold the sides. (h) Put on rubber bands to secure the sides.

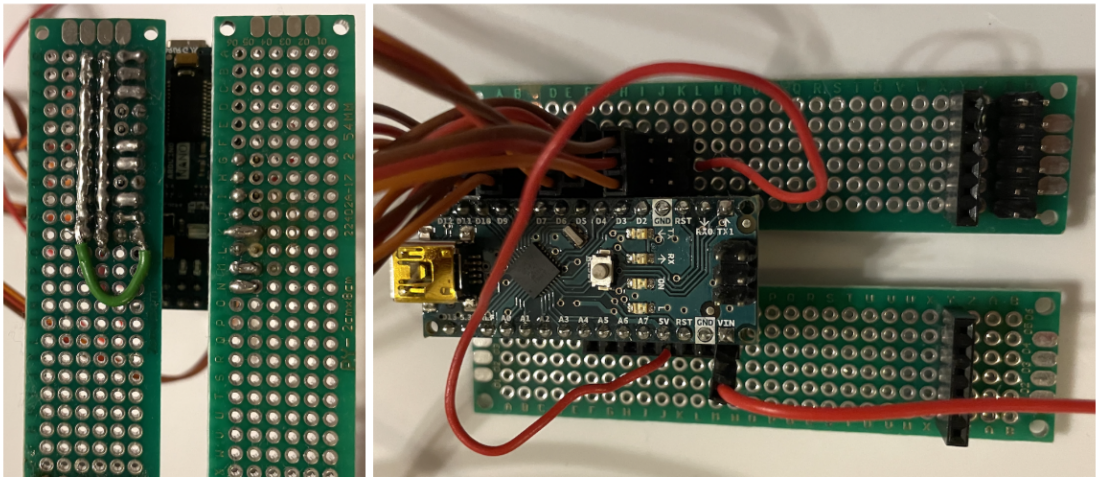

Figure 3.8: Bottom (left) and top (right) view of the TinyRHex robot control circuit board featuring modular designed hot-swap sockets to allow easily changing servo motors and Arduino without soldering and desoldering.

adapter to allow for through-hole mounting. A 2-56 thread screw accompanied by a 0.094" washer is screwed in from the previously drilled holes on the bioplastic leg and threaded through the hole drilled on the servo motor adapter. The remaining length of the screw (that pierced servo motor adapter) is then capped with a 2-56 threaded hex nut and tightened such that the connection is secure but causes no deformation to the bioplastic leg around the washer. The process and end product are shown in Figure 3.9.

After mounting all components, the weight of the TinyRhex measures around 100g (including all servo motors and bioplastic legs), and the length, width, and height of the shell measures 15 cm, 6.5 cm, and 1.3 cm, respectively. The bill of materials is included below in Table 3.3.

However, during experiments with the TinyRhex, a leg synchronization issue was discovered that would cause the robot to deviate from its original direction and veer to either the left or right side. This is extremely likely due to the six servo motors mounted on the side of the TinyRhex being out of sync.

In a correctly walking Rhex robot, the middle leg of one side of the robot should be in the exact same position as the front and rear legs of the other side. This allows the legs to alternate and push the robot forward in a straight line. However, in

Bill of materials for TinyRHex

Part	Amount	Single Price (USD)	Total Price (USD)
9V Battery	1	4.83	4.83
Arduino Nano	1	6.66	6.66
FEETECH FS90R Continuous Servo	6	5.20	31.20
Nylon Pan Head Slotted Screws 2-56 Thread, 1/2" Long	6	0.10	0.60
Nylon Hex Nut 2-56 Thread Size	6	0.10	0.60
Nylon Plastic Washer for Number 2 Screw Size, 0.094"	6	0.11	0.66
Battery Clip Connector	1	0.50	0.50
Prototype board	2	0.31	0.62
Micro Servo Adapter	6	0.75	4.5
		Total Price:	$50.17

Table 3.3: Bill of materials for TinyRHex

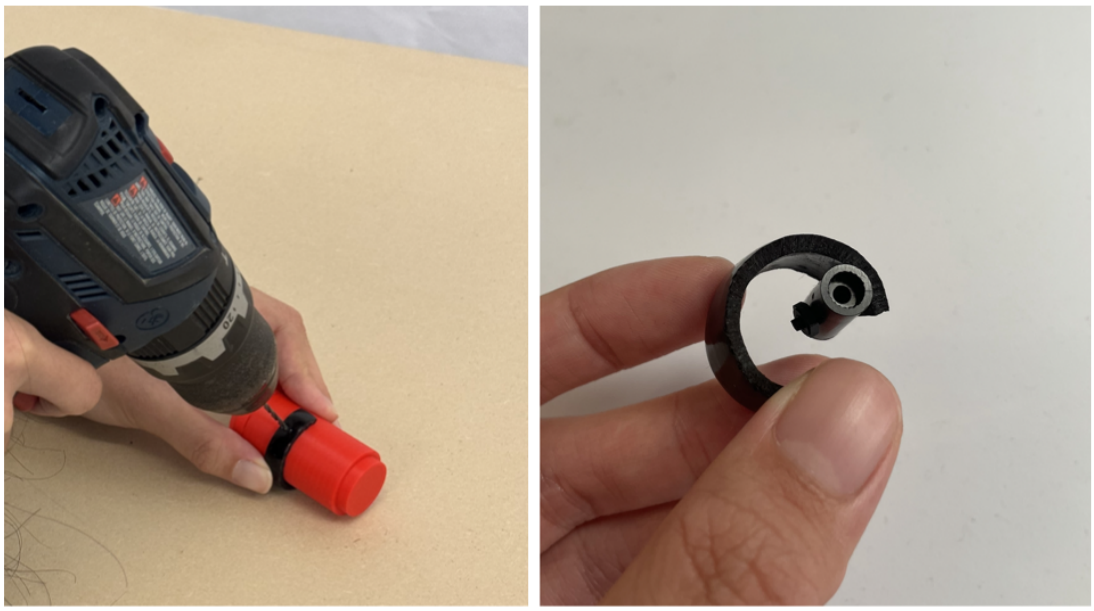

Figure 3.9: The process of attaching the micro servo adapter to the bioplastic legs so that the legs can be mounted to the output gear of the servo motor. Process of drilling the bioplastic leg (left) and attaching the servo adapter (right).

the TinyRhex robot, the FS90R continuous servo motors spin at slightly different speeds and positions due to the servo's internal tolerance issues. This breaks the synchronization in TinyRhex's designed gait pattern and causes it to veer to the side.

Several attempts have been made to remediate this issue, including motor swapping, motor calibration, and adding PID controls. Yet none of these are successful: Motor swapping does not resolve the internal tolerance issues of the FS90R continuous servos, and the issue persists even after swapping several batches. Motor calibration is done by using the slowest motor as the benchmark, and adding/subtracting constants from the other servo motor's input values in Arduino's controller code. The procedure skews the motor's actual speed and position from the Arduino's requested speed and position, and should in theory allow for all motors to be moving at the same speed. However, it was determined during repeated testing that the FS90R continuous servos tolerances were inconsistent on the same motor between runs. In particular, even with the same control signal value, a given servo motor would spin at varying speeds (with >10% deviation at times) over a continuous load interval of several seconds.

This discovery implies that it is impossible to use static calibration and open-loop control methods to synchronize the motors, and that only feedback-based closed-loop control methods (such as with PID feedback loop) are effective.

However, to apply any closed-loop control methods, rotary encoders would be required to measure the spinning speed of each servo motor. Unfortunately, there are no available rotary encoder-equipped servo motors that are small or lightweight enough to be fitted onto the TinyRhex robot. To allow for mounting any (larger) servo motors equipped with rotary encoders, the TinyRhex robot would be unsuitable, and a bigger and stronger chassis would be required.

3.2.2 MiniRhex

MiniRHex, designed by the Robomechanics Lab led by Prof. Aaron Johnson, is a miniature-scale hexapod that features a low-cost construction and fully programmable platform[3] (see Figure 3.10).

While slightly larger, heavier, and costlier than TinyRhex, MiniRhex is still rather cost-effective and compact compared to other Rhex robots (Table 3.4).

Compared to the TinyRhex discussed previously in section 3.2.1, MiniRhex has a larger chassis and is equipped with more robust and accurate servo motors with internal rotary encoders and polylactic acid (PLA) legs. Based on encoder readings, MiniRhex is able to use PD closed-loop control to synchronize the speed of each motor, thus mitigating the motor synchronization issues plaguing the TinyRhex robot.

However, due to the significantly heavier weight of the MiniRhex robot (nearly 4 times that of TinyRhex), it was soon found that the bioplastic legs previously designed for the TinyRhex robot would not be able to adequately support the weight of the MiniRhex. Thus, improvisation would be required to find a suitable method to attach the bioplastic legs to the MiniRhex.

Firstly, an attempt was made to attach the bioplastic leg layer on the outside of the original PLA legs. However, the spring coefficient of the PLA legs is measured at around 0.3 N/mm, and is approximately four times as stiff as fully dried bioplastic at only 0.072 N/mm. This high base spring coefficient provided by the PLA inner leg makes the spring coefficient changes of the composite leg (PLA inner leg attached with bioplastic outer leg) very insignificant based on moisture exposure.

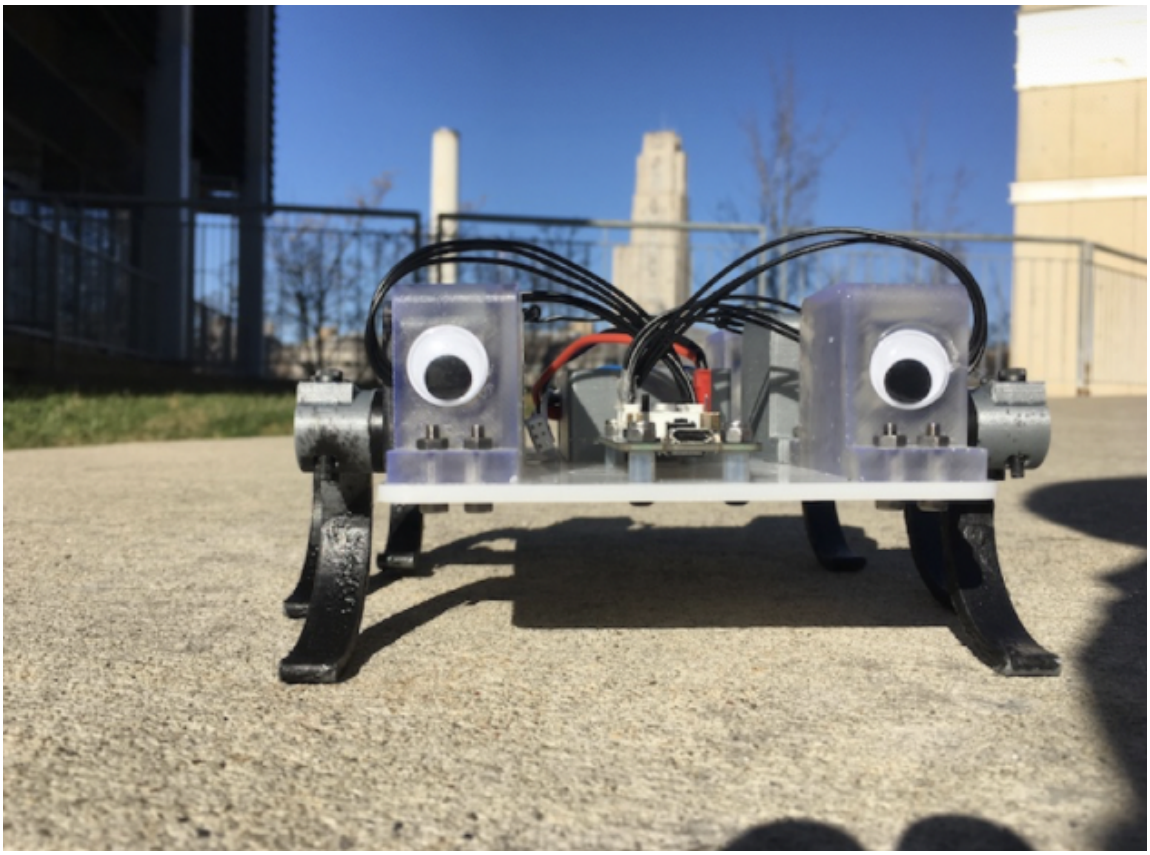

Figure 3.10: Front view of the MiniRHex Robot (Image Source: Johnson (2018)).

	Tiny RHex	MiniRHex	X-RHex (2010)
Mass	0.10kg	0.37 kg	8.6 kg
Length	0.15m	0.186 m	0.53 m
Width	0.065m	0.100 m	0.39 m
Leg Spring Constant	0.07 N/mm	0.3 N/mm	1.4-1.7 N/mm
Leg Syncing	Not Accurate	Accurate	Accurate
Leg Actuation	FEETECH FS90R Continuous Servo	Dynamixel XL330 Servo	Maxon Brushless Motor
Onboard Processor	Arduino Nano	Arduino MKR WiFi 1010	PC104, Intel Atom
Single Unit Price	~$50	~$200	~$20,000

Table 3.4: Comparison between dimensions and select specifications of TinyRHex, MiniRHex, and X-RHex (Data Source for MiniRHex and X-RHex: Robomechanics MiniRHex). Observe that MiniRhex is still rather cost-effective and compact compared to X-Rhex.

Since one of the main purposes of the legs is to be able to change stiffness according to moisture exposure, it is therefore critical that the bioplastic leg be attached to an inner support layer that is able to support the $\frac{1}{3}$ of the MiniRhex robot's weight (as there is always only three legs contacting the ground in Rhex's gait pattern) but is also of a closer spring coefficient when compared to the bioplastic leg's fully dried spring coefficient. PLA does provide adequate support but is not a good fit here due to its overwhelming stiffness. Thermoplastic polyurethane (TPU) legs were also tested, but were observed to bend excessively during gaiting tests and could not provide enough support for the robot. Finally, polypropylene (PP), a material that is stiffer than TPU but softer than PLA, is printed and tested, and found to be suitable for both its support-ability and spring coefficient.

Specifically, PP legs are printed and tested with $\frac{1}{3}$ of the MiniRhex's weight (0.37 kg). It was observed that the PP legs bend a little, but not excessively. The robot is also observed to be able to walk on a set of six PP legs normally. Additionally, the spring coefficient of the PP legs is tested via the force-displacement setup mentioned previously (in section 3.1.2). See the force-displacement diagram in Figure 3.11 below.

From the force-displacement diagram, it is observed that the spring coefficient of PP (calculated from the slope of the force-displacement curve) is 0.0701 N/mm. Note from Table 3.2 that the spring coefficient of fully dried bioplastic and bioplastic with 15 minutes of exposure in RH 75% is 0.0723 N/mm and 0.0610 N/mm, respectively. Therefore, it is concluded that the spring coefficient of PP legs lies between that of fully dried bioplastic and bioplastic with 15 minutes of exposure in RH 75%, and would serve as a good material choice to supplement the bioplastic legs in supporting the MiniRhex robot.

Yet before laminating the PP material onto the bioplastic leg, an investigation must be conducted on how thick the PP material should be for the MiniRhex to gait efficiently. We turned to nature for inspiration and found that despite differences in locomotory style, the contribution of each leg to stiffness appeared to be rather similar. Additionally, relative stiffness per leg showed a more minor variation among animals in various sizes [4], as shown in Figure 3.12 C.

According to Figure 3.12 C, the relative stiffness (k_{rel}) of the leg among trotters, runners, and hoppers always lies around 10, despite their size or weight [4]. The way to calculate the relative stiffness k_{rel} is shown below, where F is the force of

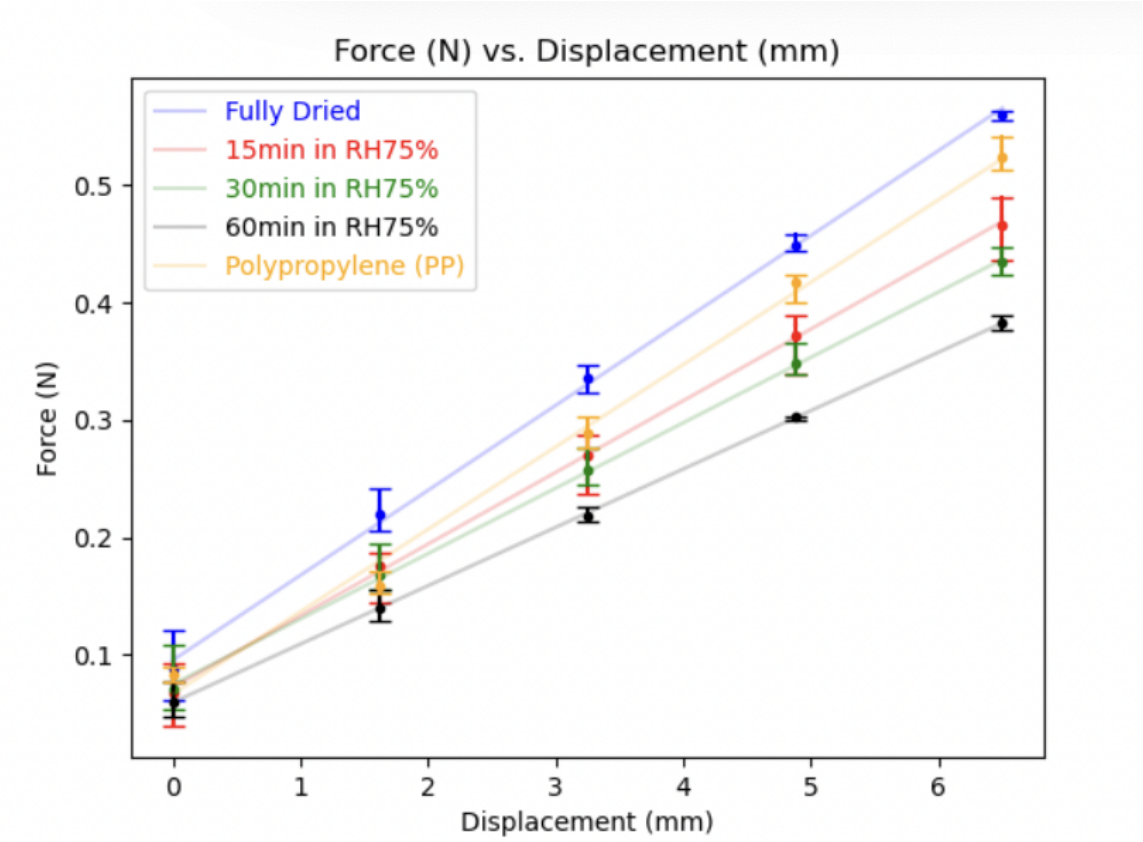

Figure 3.11: Force displacement diagram for PP and bioplastic legs with color-coded humidity condition. The slope of each force-displacement line is used to find the spring constant of each humidity and PP.

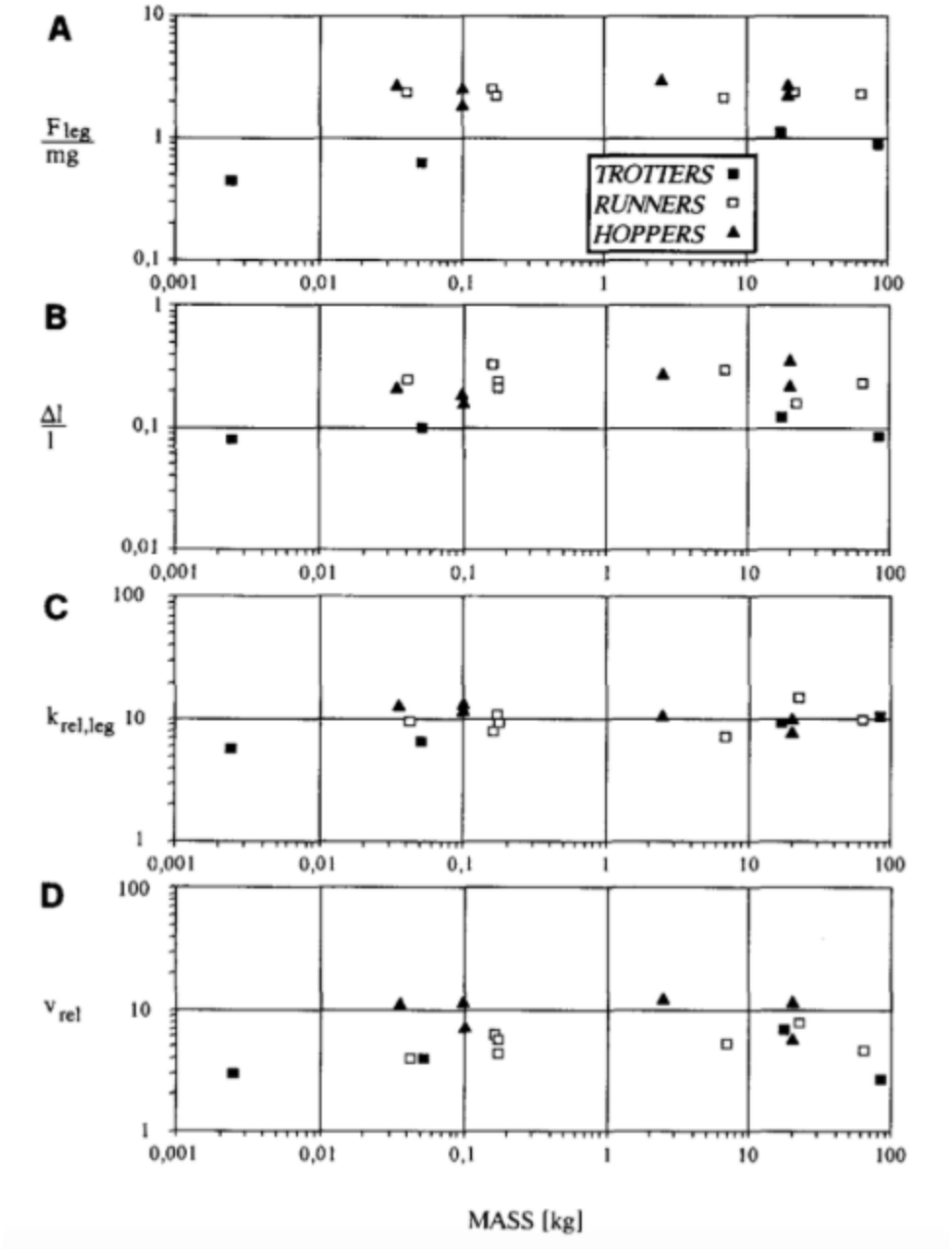

Figure 3.12: Dimensionless parameters of the monopode model for trotters, runners, and hoppers as a function of body mass. This shows that in nature, despite differences in species, the relative leg stiffness appeared to be rather similar for trotters, runners, and hoppers locomotion (Image Source: R. Blickhan and R. J. Full (1993)).

compression, m is the mass of the body, g is the gravity, l is the length of the leg, and Δl is the compression of the leg.

$$\mathrm{k_{rel}} = \frac{\frac{\mathrm{F}}{\mathrm{mg}}}{\frac{\Delta \mathrm{l}}{\mathrm{l}}} = constant$$

The gait of MiniRHex is similar to trotters, so it is reasonable to want to achieve a relative leg stiffness of around 10. Given the force-displacement result, we know $\frac{\mathrm{F}}{\Delta \mathrm{l}}$ is the spring constant we calculated earlier, we can then see what would be the best $\frac{\mathrm{F}}{\Delta \mathrm{l}}$, which is the spring constant K value that could optimize k_{rel} to be around 10.

$$K = \frac{\mathrm{F}}{\Delta \mathrm{l}}$$

$$k_{rel} = \frac{\mathrm{Fl}}{\mathrm{mg}\Delta \mathrm{l}} = (\frac{\mathrm{F}}{\Delta \mathrm{l}})(\frac{\mathrm{l}}{\mathrm{mg}})$$

Where
m: mass of the body = $0.37kg$
g: gravity = $9.8m/s^2$
l: length of the leg = $0.056m$
K: spring constant of the leg
k_{rel}: relative stiffness = 3 legs * $(K)(1000mm/m) * (\frac{0.056m}{(0.37kg * 9.8m/s^2)}) = 10$

Find K = 0.216 = $\frac{\mathrm{F}}{\Delta \mathrm{l}}$

We calculated previously that the spring constant of the fully dried bioplastic leg is 0.072368 N/mm, and the PP leg is 0.0701674 N/mm.
Thus, the optimal

$$K = 2 * K_{bioplastic} + 1 * K_{PP} = 2 * 0.072368N/mm + 0.0701674N/mm = 0.215N/mm$$

.

This means that the MiniRhex robot should be using a PP inner leg laminated with a bioplastic outer leg. The PP inner leg should have the same thickness as the original (TinyRhex) bioplastic leg, and the bioplastic outer leg should have double

the thickness of the original (TinyRhex) bioplastic leg.

To double the thickness of the bioplastic outer leg, two original (TinyRhex) bioplastic legs are laminated together with double-sided tape. Next, to attach the PP material to the inner side of the laminated double-thickness bioplastic leg, a PP inner leg was 3D printed with an Ultimaker printer following the model shown in Figure 3.13. Note that the PP inner leg was designed and printed with an integrated servo motor adapter that can be directly attached to the Dynamixel XL330 servo motor shaft. This removes the need for attaching the servo adapter, as was done previously on the TinyRHex robot.

Figure 3.13: Isometric view of the PP leg print model. Note that the printed part includes an integrated servo motor adapter, thus removing the need for attaching an external servo adapter as was done previously on the TinyRHex robot

The lamination steps are as follows (see Figure 3.14 for visual correspondence to these steps). Careful handling is encouraged to avoid any damages, tears, or misalignment.

1. Wipe the fully dried bioplastic outer leg clean using a dry paper towel.
2. Spray water uniformly on the inner and outer surfaces of the bioplastic outer leg.
3. Wait for 30 seconds and wipe clean using a paper towel until no water drop is visible on the bioplastic outer leg. Wipe hands.
4. Gently stretch the bioplastic outer leg to see if it can be formed into the same shape as the PP inner leg. Proceed if this is possible, otherwise, repeat steps 2 and 3 until the bioplastic outer leg is malleable enough.

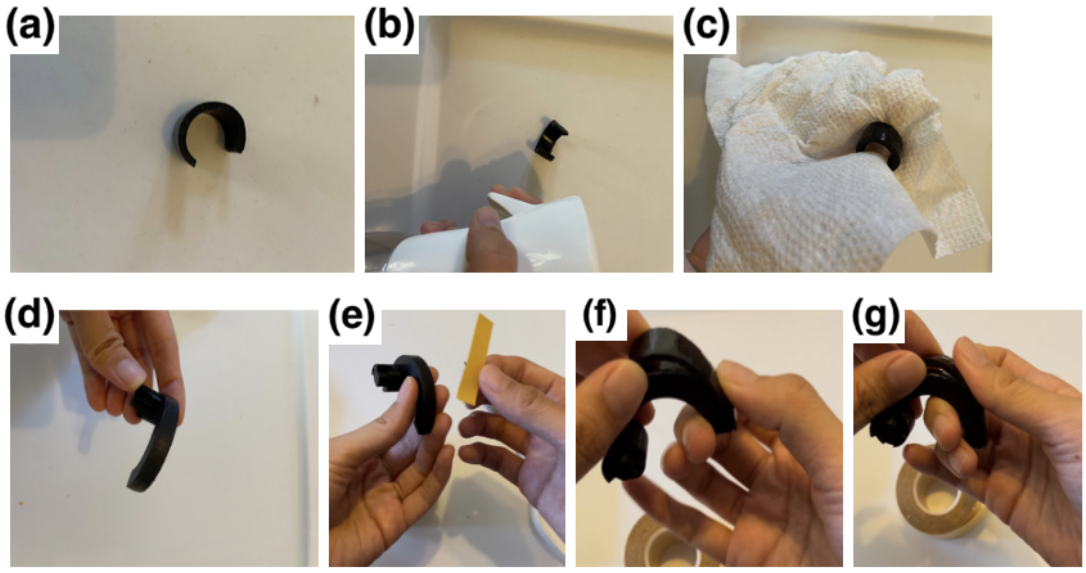

Figure 3.14: Process of laminating the bioplastic legs. (a) - (g) corresponding to the steps listed.

5. Cut strong waterproof double-sided tape (preferably 3M) to the size of the PP inner leg and attach it to the outer side of the PP inner leg.
6. Align the bottom edge of the bioplastic outer leg and the PP inner leg
7. Press down and stick the bioplastic outer leg with the bioplastic inner leg from bottom to top. Eliminate all gaps.

In order to further secure the lamination, a hole was drilled from the center of the adapter end of the PP inner leg and through the top end of the bioplastic outer leg using a size 44 drill bit. Note that the hole should pierce both the inner PP leg and the outer bioplastic leg to allow for through-hole mounting. A 2-56 thread screw accompanied by a 0.094" washer is screwed in from the outer side (bioplastic side) of the previous drilled hole and threaded through the inner side (PP side). The remaining length of the screw (that pierced the PP inner leg) is then capped with a 2-56 threaded hex nut and tightened such that the connection is secure but causes no deformation to either the bioplastic surface around the washer or the PP surface around the hex nut. The process and end product are shown in Figure 3.15.

Figure 3.15: Laminated bioplastic leg after performing steps in Figure 3.14

3.2.3 Sensor Exploration

In addition to the robot development, we also explored humidity sensors to pave a path for future testing and experimentation in a real-world environment. When testing in the lab, we could use the humidity chamber to create the exact humidity needed, but when we are out in the natural environment, we would need sensors to keep track of the humidity. We found a way to successfully transmit the humidity data wirelessly through the wifi, and we hope this could help future researchers when they perform experiments with the MiniRhex and bioplastic legs in natural environments.

After careful consideration, we have decided to use the RH-NRF24 chipset for wireless transmission and the DHT-22 Humidity Sensor Chip for humidity measurement. RH-NRF24 is an easy-to-use and cost-effective RF communication chip that allows two identical NRF24s to communicate as sender and receiver. It is suitable for our use case as we do NOT require long-range communication and have no safety concerns or strong interference resilience requirements. It is also compatible with Arduino (boards with SPI Hardware interface implementation and support) and is supported by the Radiohead Opensource Arduino Library.

DHT-22 Humidity Sensor Chip is an easy-to-use and cost-effective capacitive humidity sensor. It is suitable for our use case as it is compatible with Arduino and requires very little setup to get relatively accurate humidity readings (+/- 2%, but

specification varies depending on the supplier).

Previously (before the above sourcing finalizations), we have attempted to use DHT-11 Humidity Sensor Chip and XBee WIFI Transmitter.

- DHT-11 Humidity Sensor Chip: The chips we sourced failed due to unknown reasons (suspected lack of manufacturing quality). We are unable to get any readings.
- XBee WIFI Transmitter: The chips we sourced failed due to an internal short, resulting in severe damage to the XBee chip itself and an Arduino Uno. Sparks and hazardous smoke were observed at the time of connection. We choose to not use these due to health and safety concerns.

To set up the sensors and RF transmission, we first need to set up the circuit and wiring for the component. The following wiring diagram must be connected as is. The RH-NRF24 chipset (transmitter and receiver) communicates with the Arduino hardware interface using the Serial Peripheral Interface (SPI). Due to limitations of the SPI implementation on the Arduino hardware interfaces, SPI ports are hardcoded in hardware construction and cannot be moved. Should these ports be moved in the programming or connection, the SPI communication will not function correctly, and messages cannot be transmitted and received.

Transmitter (with RH-NRF24 RF Communication Chip and DHT-22 Humidity Sensor Chip)

RH_NRF24/CE <==> Arduino/D8
RH_NRF24/CSN <==> Arduino/D10
RH_NRF24/SCK <==> Arduino/D13
RH_NRF24/MOSI <==> Arduino/D11
RH_NRF24/MISO <==> Arduino/D12
RH_NRF24/VCC <==> Arduino/3.3V
RH_NRF24/GND <==> Arduino/GND
DHT_22/VIN <==> Arduino/5V
DHT_22/OUT <==> Arduino/DHT22_PORT_AS_DEFINE_IN_CODE
DHT_22/GND <==> Arduino/GND

Receiver (with RH-NRF24 RF Communication Chip)

RH_NRF24/CE <==> Arduino/D8

```
RH_NRF24/CSN <==> Arduino/D10
RH_NRF24/SCK <==> Arduino/D13
RH_NRF24/MOSI <==> Arduino/D11
RH_NRF24/MISO <==> Arduino/D12
RH_NRF24/VCC <==> Arduino/3.3V
RH_NRF24/GND <==> Arduino/GND
```

Additionally, ensure the Arduino boards get sufficient power to ensure stable and adequate voltage for connected components. Ensure to NOT substitute 5V and 3.3V ports for each other. - Using 3.3V to power the DHT-22 Humidity Sensor chip may lead to inaccurate readings if the chip is not rated to work for 3.3V DC. Please check the supplier specification. - Using 5V for powering RH-NRF24 will cause severe chip damage, fires, and expose users to risks of inhaling materials that may lead to Cancer and reproductive harm.

After completion of the wiring and connections, we can compile and upload the code in Appendix A to the transmitter and receiver Arduino.

Note that compilation of the above code is dependent on the installation of the Arduino Radiohead Opensource library for dependencies on RF transmission. To install, ensure you have an internet connection, boot into Arduino API, and perform the following steps:

```
Arduino > Sketch > Include Libraries
> Manage Libraries > Library Manager
> Search RadioHead > Install
```

Make sure you restart the IDE after installation. You should now be able to compile and upload the code above.

You can observe the transmissions from the Serial Monitor in the Receiver Arduino when it is connected to the Arduino IDE. The transmissions should be in the form of:

```
Incoming message intercepted...
humidity_value is 50
```

Chapter 4

Robot Experiment

From the inspiration of amphibia and previous research on RHex robot's stiffness changing studies [15] as described earlier in Chapter 1, we want to learn the performance of the bioplastic legs on MiniRHex in different humidity environments and terrains. With this goal in mind, we performed 4 tests, including test aspects of friction, incline, aqua, and foam.

- Friction Tests: Quantitative analysis regarding the static friction of the robot when moving on a rigid surface for different humidity. (section 4.1)
- Incline Tests: Quantitative analysis regarding the maximum slope of rigid incline the robot is capable of climbing repeatably, under different lengths of humidity exposure of the bioplastic wheels. Also measures these metrics under different incline conditions (such as wet incline surfaces) and other wheel materials (PP/PLA). (section 4.2)
- Foam Tests: Quantitative analysis on robot's performance on soft surfaces (foam) when tested under different lengths of humidity exposure of the bioplastic wheels. Also tests these metrics with PLA and PP leg materials. (section 4.3)
- Aqua Tests: Qualitative analysis regarding how well the bioplastic leg moves like a fin when partially submerged in water when compared to the original PLA leg. This implies the robot's amphibious abilities when scaling waterous terrain. (section 4.4)

From these experiments, we found that the dried and stiff bioplastic legs results in

better performance on softer surfaces (e.g. foam), and the wet and soft bioplastic legs have higher friction (especially when wet) and result in a better performance on inclines and water.

4.1 Friction Tests

This test aims to see how static friction between the robot's legs and the rigid ground (wooden board) changes with respect to humidity/water exposure. This test shows that as the humidity exposure increases, the robot with bioplastic legs has a larger friction coefficient compared to bioplastic legs in dried condition and legs constructed in two other materials, PP and PLA.

4.1.1 Simple Qualitative Tests

We used a simple force sensor to see if there was any significant difference between the friction characteristics of the dried and the wet bioplastic legs, as shown in Figure 4.1 a. We first tested the fully dried legs, and then put the legs in water for 1 minute, wiped dry and re-tested with the same procedure. We are able to see a 2.5 times difference from the readings between these two conditions, as shown in Figure 4.1 b and c.

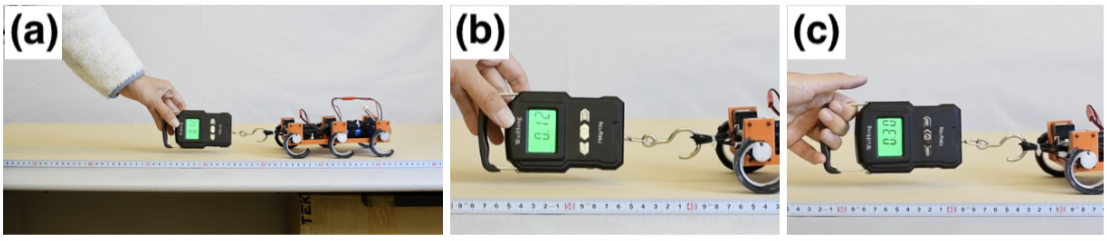

Figure 4.1: Simple Qualitative Test to determine if there was any significant difference between the friction characteristics of the dried and the wet bioplastic legs. (a) Setup. (b) Force reading of fully dried legs. (c) Force reading of wet legs immersed in water for 1 min.

Thus, we determined that there is a significant enough difference between the friction of fully dried legs versus legs exposed to water. However, since the forces tested are near (and at times below) minimal accurate force measurable with the

WeiHeng force sensor, we are not able to fully guarantee the accuracy of the force readings. To obtain more accurate data, we changed to more accurate force sensors (i.e. load cells) and measured for longer durations (section 4.1.2).

4.1.2 Accurate Quantitative Tests

In this experiment, we performed the friction test with a more accurate setup and a wider range of humidity levels and exposure methods. The setup is shown in Figure 4.2, where we attached a Transducer Technology GSO series 500g load cell to a white PLA hand holding block with an extruded bar, and used an LCA-RTC load cell amplifier along with an Arduino UNO to read the values to the laptop. The extruded bar would be blocked by a pre-measured trail for every 5 cm of pulling to eliminate errors. We manually pull the block horizontally with minimum force that would be able to drag the robot forward at a constant velocity while making sure the bottom of the block is slicing on the platform.

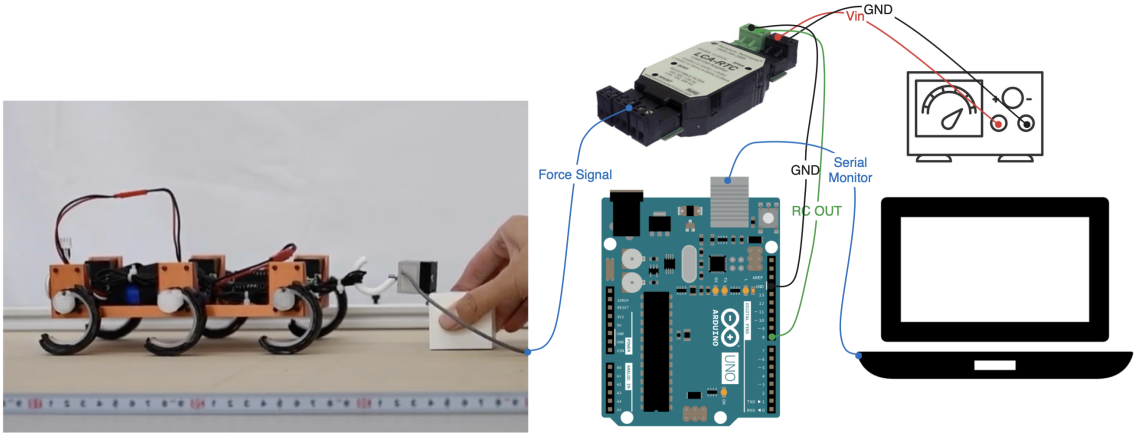

Figure 4.2: Setup of the accurate quantitative tests to determine friction characteristics differences of PP, PLA, dried and wet bioplastic legs.

In each trial, we pull the MiniRHex 10 times, each time the robot moves for 5 cm at a constant velocity. We performed 5 trials to get a total of 50 data points for each humidity level for the bioplastic, along with baseline testing for PP legs and PLA legs. The humidity chamber was set to 75% RH and temperature of 25°C. The test was conducted when the bioplastic legs were fully dried, and placed in the chamber for 15 min, 30 min, and 60 min. We also conducted the same test for water dipping,

in which the MiniRHex stood in 2 mm water ($\frac{1}{2}$ of 1 leg thickness) for a set duration of time, was padded dry using a paper napkin, and tested immediately. The duration of submersion time for wet testing is respectively 1 min, 2 min, 3min, and 5min. The results for both dry, humidity chamber exposure, wet, and PLA/PP are shown in Figure 4.3.

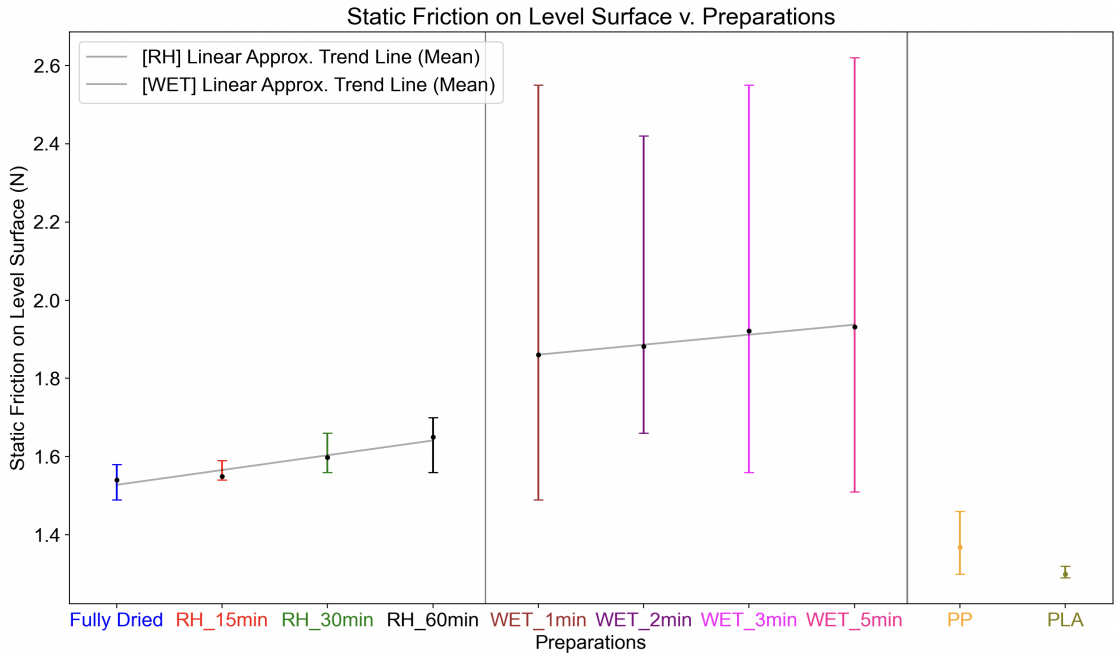

Figure 4.3: Static friction on level surface vs. Preparation diagram for dry, humidity chamber exposure, wet, and PLA/PP legs. See detailed analysis in section 4.1.2

For friction changes in water dipping (WET_Nmin), we found that dipping in water increases the friction coefficient of the bioplastic legs significantly for a short duration. We suspect that this increase in surface coefficient can be attributed to several factors: an increase in surface contact patch due to a decrease in material stiffness (i.e. softer material makes "flatter" and more cohesive contact with ground/surface), and an increase in surface cohesion or stickiness (i.e. the material becomes more sticky when wet, instead of slippery). To quantitatively analyze the contribution of either of these factors, we would need to rely on microphysics and tribology. We will thus refrain from such discussion as it is out of the scope of this project, but we still recognize it as an interesting direction of future study for physicists and material scientists.

For friction change in the humidity chamber (RH_Nmin), we see that the changes

in friction coefficient are present, but significantly smaller compared to that of dipping in actual water. We believe that the change in friction coefficient (after humidity chamber exposure) is caused by tiny atmospheric water droplets (due to high relative humidity) colliding with bioplastic when in humid environments and being absorbed by the bioplastic's surfaces. Moreover, the changes in friction coefficient is smaller than when dipped in water, as the bioplastic absorbs much less water during environment droplet collision (in RH 75%) when compared to being submerged in water.

By analyzing the data, we also discovered that in all scenarios where the bioplastic legs are exposed to moisture or water, the legs would exhibit much higher friction coefficient initially, but the friction coefficient would soon decrease and eventually (through continuous testing with the setup mentioned above) decrease to the point of matching the friction coefficient of the dried bioplastic legs (Figure 4.4). We attribute this change to the bioplastic material slowly drying up during the process of testing, as the friction force (by dragging MiniRHex across the table repeatedly) generates heat and therefore quickly dries up the surface layer of the bioplastic material.

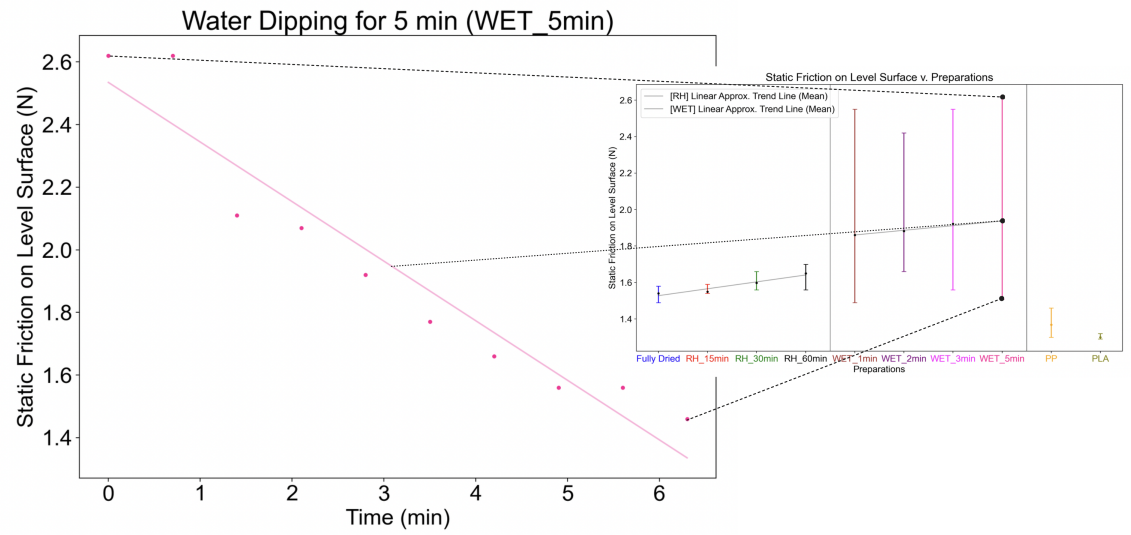

Figure 4.4: Water dipping for 5 minutes data plot with the trendline. Showing that the legs would exhibit a much higher friction coefficient initially, but the friction coefficient would soon decrease due to friction drying the bioplastic surface, and eventually decrease to match the friction coefficient of the dried bioplastic.

4.2 Incline Tests

In order to see how the rigid surface performance of the robot changes with respect to humidity, we conducted this incline test to simulate the robot's ability to traverse rough terrain. The first part of this test shows that as the exposure to humidity increases, the MiniRHex with bioplastic legs could climb a higher slope on the dried rigid wood incline compared to the dried condition and two other materials, PP and PLA. The second part of this test shows that when the incline is wet, MiniRHex with the bioplastic legs performs better than compared to dry conditions, while the performance of MiniRHex with the PP legs decreases in the same (wet) condition when compared to their respective performance in dry conditions.

4.2.1 Dried Incline Tests

We conduct this incline test to see the relationship between the duration of humidity/water exposure of the legs of the MiniRHex and the largest possible slope the robot is able to climb on a dried rigid surface. We attached a measuring tape on the side of the platform, along with a protractor to measure the angle of slope. We ensured that the setup was rigid, stable, and the slope was straight and not sagging during robot movements. An example of the setup is shown in Figure 4.5.

During testing, we slowly increment the angle of incline (with a precision of 1 degree) to determine the maximum angle the robot is able to climb up at each respective humidity/water exposure. The test was conducted 5 times when the bioplastic legs were fully dried, and placed in the chamber for 15 min, 30 min, and 60 min. The humidity chamber was set to 75% RH and temperature of 25°C. The bioplastic legs were taken out of the chamber and immediately installed and tested on the inclines (within 3 minutes of taking out of the chamber), with the robot attached to a fully charged battery each time. We also include the baseline testing for PP legs. The results are shown in Figure 4.6.

From this result, we noticed a small but positive difference for the maximum climbable incline between each humidity exposure interval. We also found that bioplastic legs perform better than PLA legs regardless of levels of exposure.

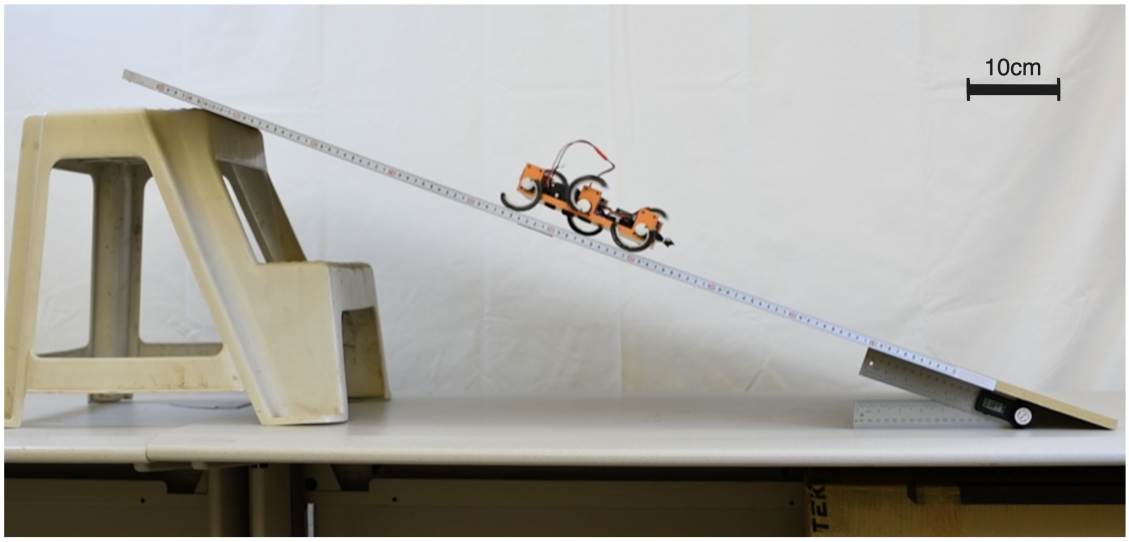

Figure 4.5: Setup for incline tests to find the relationship between the duration of humidity/water exposure of legs of the MiniRHex and the largest possible rigid slope the robot is able to climb. The configuration demonstrates MiniRHex successfully climbing an 18-degree angle on a rigid wooden incline surface.

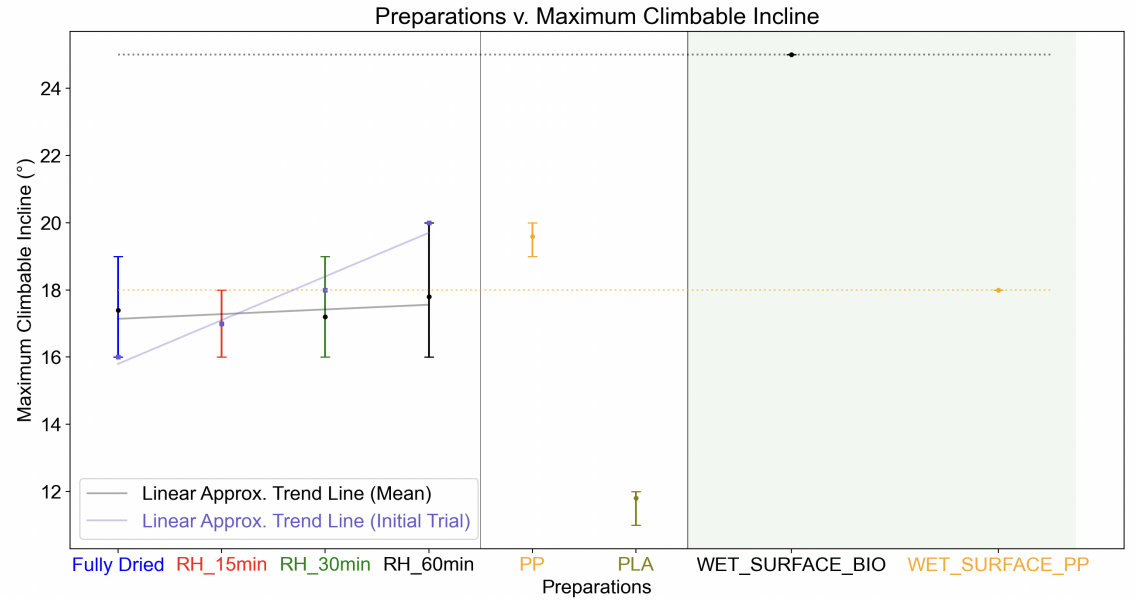

Figure 4.6: Incline test result. Left: Dried incline test for MiniRHex with bioplastic legs with respect to time in RH 75% humidity chamber. Middle: Baseline dried incline test for MiniRHex with PP and PLA legs. Right: Wet incline test for bioplastic and PP legs.

4.2.2 Wet Incline Tests

We also conducted the wet incline test to test the performance of different legs by simulating a wet and slippery condition on the incline. From the friction testing, we suspect that the wet surface could in fact add traction to the bioplastic legs, which is beneficial because robot locomotion usually has difficulties when maneuvering on wet terrains as the water makes the surface slippery. We used the same setup for this experiment, as shown in Figure 4.5. To create a rainy environment, we sprayed water using a continuous spray bottle uniformly on the platform for 30 seconds. The spray bottle we used has an output of 35 ml/min (+/- 2.5ml). We performed the same experiment on the robot with the bioplastic legs and PP legs, the result is shown in Figure 4.6. We noticed that the performance of PP legs dropped from 20 degrees (dried incline) to 18 degrees (wet incline). We believe that the PP legs performed worse on the wet incline because the simulated rain made it more slippery and thus caused the PP legs to lose traction. On the other hand, we found that the robot with bioplastic legs is able to climb up to 25 degrees (wet incline) as compared to the maximum of 20 degrees (dried incline). Moreover, the robot is able to perform 38.9% better on the wet surface with bioplastic legs compared to PP legs.

In conclusion, the MiniRhex with bioplastic legs has better performance than the PP and PLA legs, especially in wet environments and slippery surface conditions.

4.3 Foam Tests

We conducted the foam test to study how the soft surface performance of the robot changes with respect to humidity exposure. This test shows that as the humidity decreases, the MiniRHex with bioplastic legs has a higher average speed (thus takes shorter to walk a specific distance) when walking on a soft surface. This test also shows that the MiniRHex is able to walk on the foam surface with bioplastic legs, but is not able to walk on the foam surface with the two other leg materials, PP and PLA.

The foam we are using is a super soft foam with 6 inches of thickness. The indentation load deflection (ILD), a way to measure the firmness of the foam, is 12 lb for the foam we tested on. We attached a measuring tape on the side of the foam.

The experiment setup is shown in Figure 4.7.

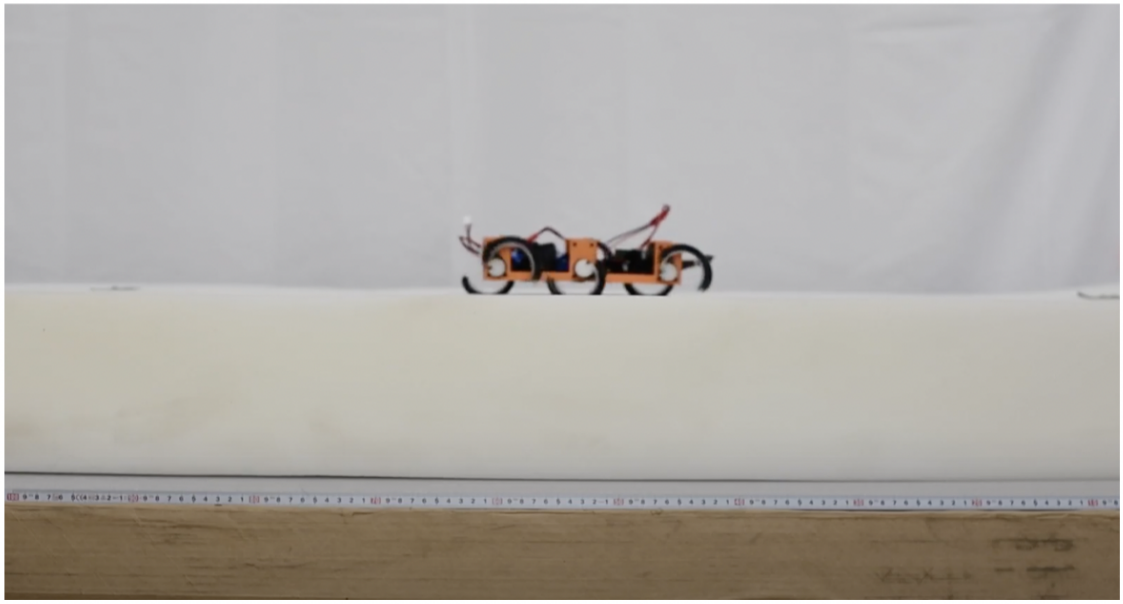

Figure 4.7: Setup for foam test to study how the soft surface performance of the robot changes with respect to humidity exposure.

We first tested and compared the fully dried bioplastic legs and bioplastic legs exposed in 75% RH humidity for 30 minutes, with 5 iterations of each material and condition. The velocity of the MiniRHex with fully dried bioplastic legs is 14.3 cm/s, and the velocity for 30 minutes in 75% RH bioplastic legs is 12.5 cm/s. This shows that the dried bioplastic legs performed better than the semi-wet bioplastic legs (30 minute RH75 % exposure). However, since the difference between the velocities is not significant (about 12.6%), instead of putting the legs in a humidity chamber, we decided to immerse the leg in water for 1 minute and 5 minutes and perform the same test immediately after immersing. First, we prepared a bucket of water and made sure the bioplastic legs were fully submerged. After the corresponding duration, we took them out and wiped them dry using paper towels, and then performed the same experiment immediately on the MiniRHex with these legs. From this experiment, we found that the velocity of the MiniRHex with 1 minute water immersed bioplastic legs is 10.6 cm/s, and the velocity for 5 minutes water immersed bioplastic legs is 9.3 cm/s. There is a 35% increase between the 5 minutes water immersed bioplastic legs

and the fully dried legs in terms of velocity on soft foam. This shows that the dry bioplastic legs performed better than the wet legs on the soft foam surface.

In addition, we also tested the PP and PLA legs on the soft foam surface. To our surprise, neither of these legs is able to walk on the foam surface. We observed that in both PP and PLA cases, the legs would rotate in the beginning for only several rotations, but would quickly become stuck inside the soft foam surface and the motors are not able to produce enough continuous torque to unstuck the robot (at least not without triggering the over-current protection system built into the servo motors). We tested 5 times for each of the PP and PLA legs, and the results were consistent across all trials.

The comparisons are shown in the Table 4.1.

Leg	Speed
Fully Dried Bioplastic	14.3 cm/s
30 minutes in the 75% RH	12.5 cm/s
1 minutes immerse in water	10.6 cm/s
5 minutes immerse in water	9.3 cm/s
PLA	Not working
PP	Not working

Table 4.1: Speed comparison for foam testing with corresponding legs attached to MiniRHex

Based on the earlier research on leg stiffness of RHex robot [4], we predicted theoretically that the bioplastic legs would perform better than the PP legs, as they are stiffer. However, PLA legs are much stiffer than the bioplastic legs, but bioplastic legs also perform better than the PLA legs.

Therefore, we suggest that there might be a leg stiffness threshold when moving on a soft surface, such that only legs within the threshold would be able to traverse the surface (while following the stiffness-speed correlation previously discussed [4]), and that legs that fell outside this threshold would get stuck and not be able to move

at all. We further suggest that this leg stiffness threshold is determined by various factors, including but perhaps not limited to motor torque rating, surface softness (measured in ILD), and leg mounting methods. It seems that our bioplastic legs fell within the stiffness threshold, while the PLA and PP legs did not.

We will not be making a quantitative argument regarding this stiffness threshold here as it is out of scope for this project but would note that this finding does open up a new research question for future studies.

In conclusion, we find that the MiniRhex with bioplastic legs has better traverse performance (traverse speed) than the PLA and PP legs on softer surfaces, especially in dry environments.

4.4 Aqua tests

In order to achieve our ultimate goal of making an amphibious robot, we were also curious about how the bioplastic legs could benefit the performance of water operations, such as swimming. We therefore conducted this aqua test using a single bioplastic layer of the bioplastic leg that was previously designed to be used on TinyRHex (as described in section 3.2.1). This test aims to show that the bioplastic legs are able to be more flexible in water and are thus more suitable for in-water locomotion than rigid PLA legs.

The setup is shown in Figure 4.8. We created a water tank and attached a servo motor to the surface of the water. We then attached the leg on the servo motors and connected the servo motor to an Arduino to produce a constant speed continuous counterclockwise movement. We drop food dye on top of the servo rotation pivot and observe the expansion speed of the food dye in water with respect to legs made with different materials.

We tested PLA leg and bioplastic leg when submerged in water for 3 minutes, 5 minutes, 10 minutes, and 30 minutes. We collected photos for 0 seconds, 5 seconds, and 10 seconds after dropping the food dye into the water. The results are shown in Figure 4.9.

From the pictures, we observed that the bioplastic legs, especially after a longer period of submersion in water, are able to push the food dye away horizontally further than the PLA legs. The bioplastic leg gets softer when placed in water for longer,

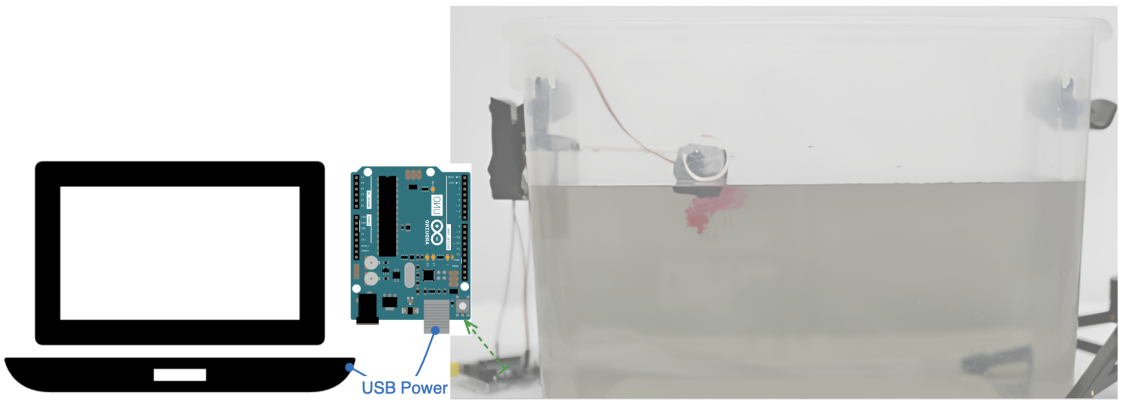

Figure 4.8: Setup for aqua testing to determine the performance of bioplastic legs in water operations, such as swimming.

and when we use servo motor to thrust the leg in water, we observe a deformation of the bioplastic while the water contacts it, as shown in Figure 4.10. This tendency to deform easily allows the leg to behave like a fin, which influences the fluid dynamics around the robot and allows the swimming motion of the robot to be more effective.

In conclusion, this test shows that the bioplastic legs are able to be more flexible in water and are thus more suitable for in-water locomotion than rigid PLA legs.

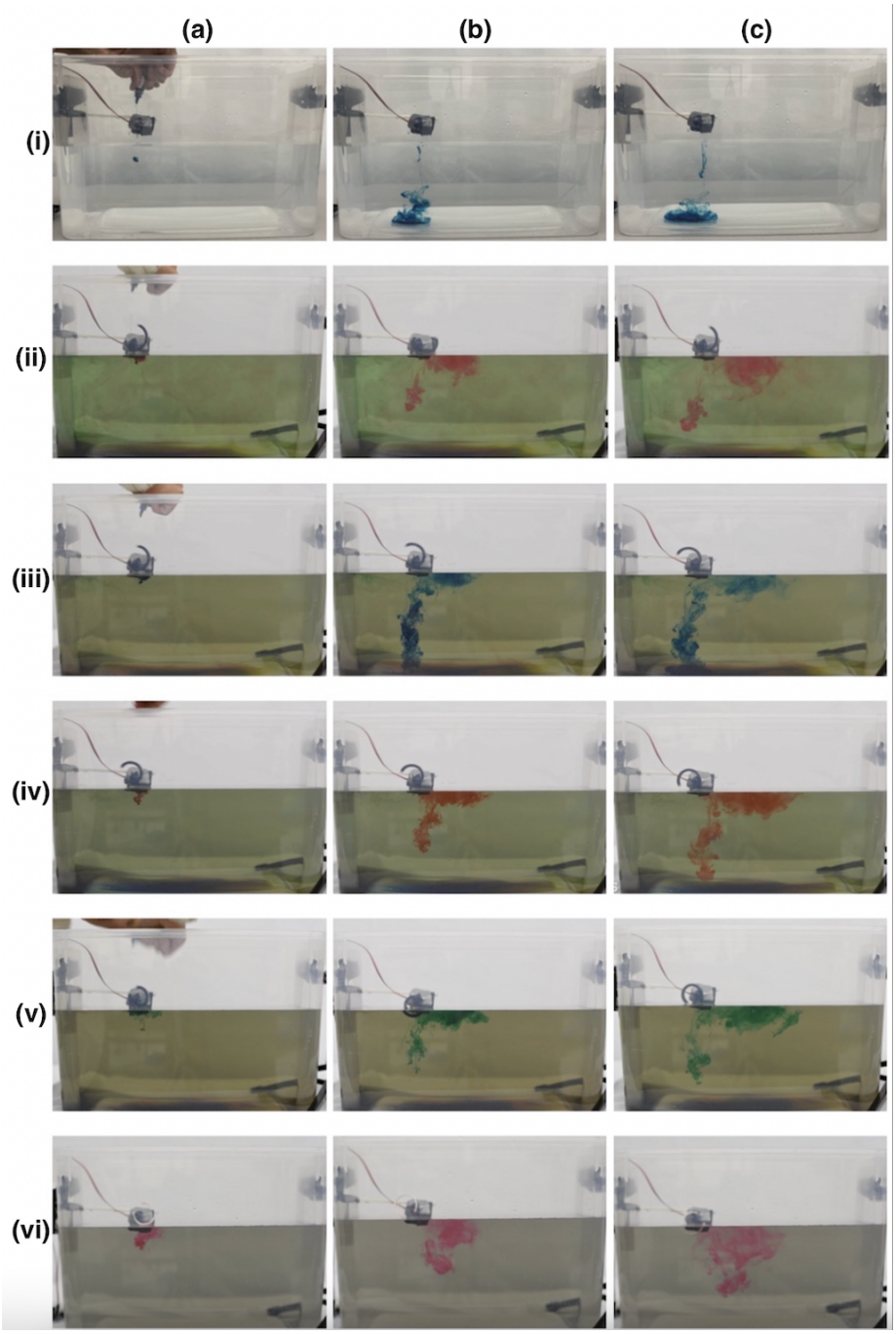

Figure 4.9: Aqua Test result. Row (i): baseline test with only food dye. From row (ii) to row (vi): bioplastic leg when 3 minutes, 5 minutes, 10 minutes, and 30 minutes in water, PLA leg. From (a) to (c): 0s, 5s, and 10s after dropping the food dye. Observe that the bioplastic legs, especially after a longer period of submersion in water, are able to push the food dye further away horizontally than the PLA legs.

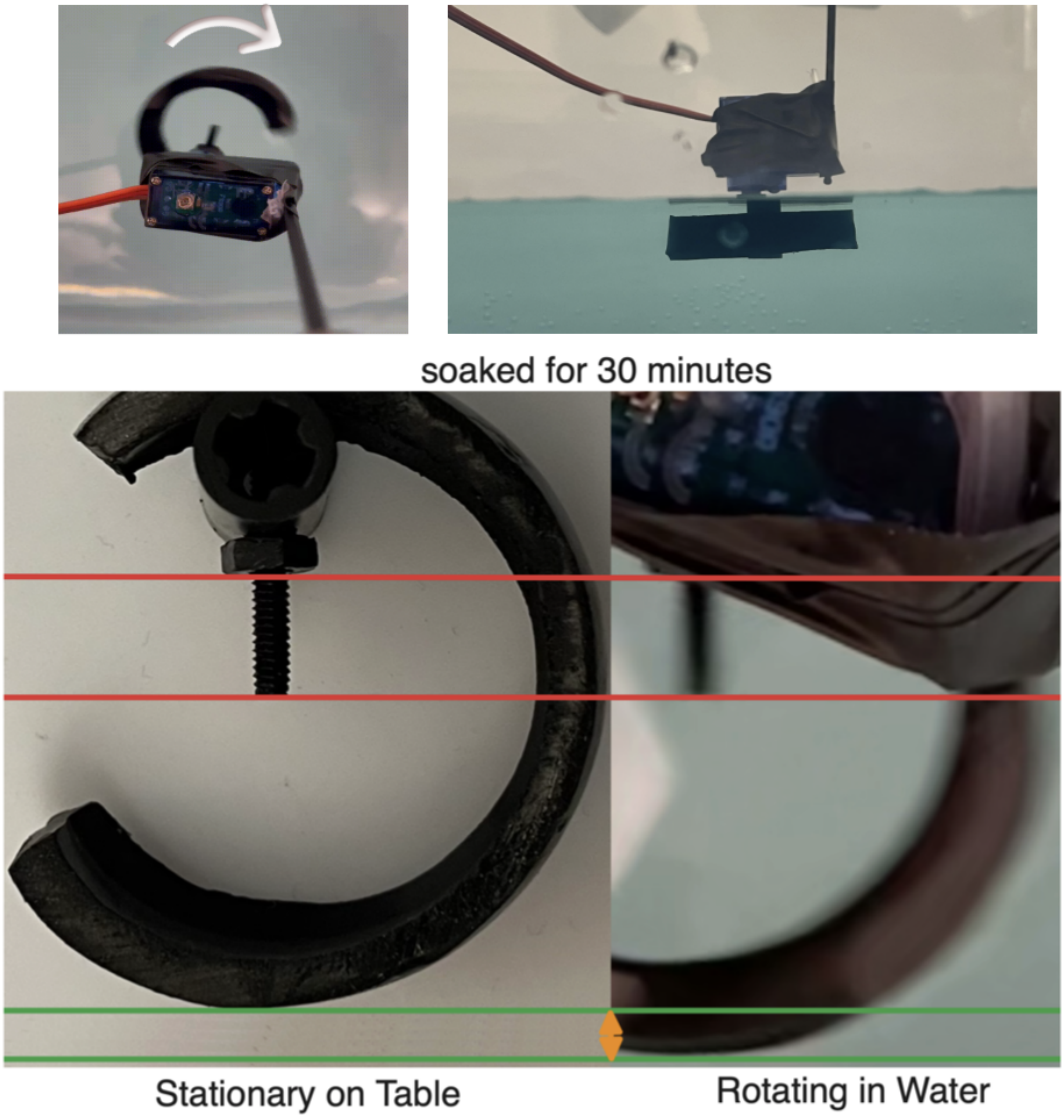

Figure 4.10: Deformation in water. Upper row: top view (left) and side view (right) of the bioplastic leg fully immersed in water and connected to a servo motor. The servo motor rotated clockwise in the water, and the bioplastic was soaked in water for 30 minutes. Bottom row: an expansion of the bioplastic leg was observed as it moves in water. We use the length after the hex nut as a reference (red), and the bioplastic leg expands (green) to achieve a length difference (orange). This expansion results in a larger surface area, which could potentially enhance its ability to resist water and improve performance when flapping in water.

Chapter 5

Conclusion and Next Steps

5.1 Conclusion

In this thesis, we presented the material development, fabrication techniques, and fabrication process for an innovative material, bioplastic, to be used as legs on RHex robots in order to achieve better locomotion. By conducting a characterization analysis for the bioplastic legs, including stability test and force-displacement test, we understand how the bioplastic leg responds to different humidity levels, and thus able to be used for contributing towards our ultimate goal of developing efficient amphibious robots.

After mounting the bioplastic legs onto the MiniRHex robot, we presented four tests to illustrate the change in performance of the MiniRHex with respect to leg materials, conditions, and environments. The friction test shows the friction of the MiniRHex with bioplastic increases with longer exposure to moisture and/or water. The incline test shows that the MiniRHex with bioplastic legs is able to climb a higher incline with longer exposure to moisture and/or water. This test also shows that in a slippery environment, such as rainy days, the bioplastic legs have better performance over conventional materials such as PP and PLA.

While the first two tests show that in wet conditions, the MiniRhex with bioplastic legs has better performance than the original PLA legs, the foam test shows that the bioplastic legs also perform better in dry conditions when overcoming very soft terrains (e.g. foam). The MiniRHex with PLA legs are unable to move on soft foam

surfaces, but with the bioplastic legs, the robot is able to move on the soft foam and perform better, especially in low-humidity environments.

We concluded that in wet environments, the MiniRHex with bioplastic legs has higher friction on a rigid wood surface and could perform better on inclines than the PLA legs. In dry environments, the MiniRHex with bioplastic legs could perform better when overcoming soft foam surfaces and also result in better performance than the PLA legs.

In addition to these results, we also conducted the aqua test to find out that the bioplastic legs may potentially enhance the swimming performance of the robot, which provides a starting point for future research to develop amphibious robots with bioplastic. Moreover, we also provide a method to transmit the humidity data of the environment wirelessly after exploring humidity sensors.

5.2 Future Research

Moving forward, future research could utilize our results to further detail the performance of the robot with bioplastic legs in natural environments with different humidity, and eventually contribute to the development of efficient amphibious robots with bioplastic material.

In our robot experiments, we made interesting observations regarding the performance of bioplastic legs in friction and foam tests. The friction test revealed that the bioplastic legs demonstrated superior performance on wet surfaces, which contrary to the usual expectation that wet surfaces are more slippery and would lead to lower performance of the robot legs due to lower friction. Moreover, during our foam testing, we found that the stiffer PLA legs failed to traverse the foam while the softer bioplastic legs are able to traverse effectively on foam. The investigation of the underlying reason for this unexpected behavior is out of scope for this study, but could be a good subject for further research and analyzing. Thus, one direction of the future research could be understanding the physics underlying both the friction and foam test results in order to gain a more comprehensive understanding of how leg design and material properties influence performance in various environmental conditions.

In addition, to enable seamless navigation through real-world environments, future

research could equip the robot with a variety of sensors for automation operations, such as cameras, LiDAR, and humidity sensors. Furthermore, an in-depth exploration could be conducted for refining and enhancing the performance of bioplastic legs in real-world environments. Future endeavors could prioritize the development of a nuanced understanding of how bioplastic legs respond to the dynamic conditions encountered in real-world scenarios. By subjecting the bioplastic legs to a range of real-world challenges and field tests, we aim to uncover material advantages and limitations that may not be apparent in the controlled lab settings. With this understanding, we may be able to refine the material composition and incorporate more adaptive features to optimize the legs to achieve better performance for practical future robotics applications.

Appendix A

Transmitter and Receiver Code

A.1 Transmitter

(with RH-NRF24 RF Communication Chip and DHT-22 Humidity Sensor Chip)

```
#include <SPI.h>
#include <RH_NRF24.h>
#include <DHT.h>

#define DHT22_PORT_AS_DEFINE_IN_CODE 7

RH_NRF24 nrf24;
DHT dht(DHT22_PORT_AS_DEFINE_IN_CODE, DHT22);

void setup()
{
  Serial.begin(9600);
  dht.begin();

  if (!nrf24.init())
    Serial.println("init failed");
  if (!nrf24.setChannel(1))
```

```
    Serial.println("setChannel failed");
  if (!nrf24.setRF(RH_NRF24::DataRate2Mbps, RH_NRF24::TransmitPower0dBm)
    Serial.println("setRF failed");

  Serial.println("init done");
}

void loop()
{
  int humidity_value = dht.readHumidity();
  uint8_t data_str[16];
  sprintf(data_str, "\%d", humidity_value);

  Serial.print("Sending humidity value: ");
  Serial.print((char*)data_str);
  Serial.println("...");

  nrf24.send(data_str, sizeof(data_str));
  nrf24.waitPacketSent();

  Serial.println("Message Sent Successfully\n");
  delay(1000);
}
```

A.2 Receiver

(with RH-NRF24 RF Communication Chip)

```
#include <SPI.h>
#include <RH_NRF24.h>

RH_NRF24 nrf24;
```

```
void setup()
{
  Serial.begin(9600);

  if (!nrf24.init())
    Serial.println("init failed");
  if (!nrf24.setChannel(1))
    Serial.println("setChannel failed");
  if (!nrf24.setRF(RH_NRF24::DataRate2Mbps, RH_NRF24::TransmitPower0dBm))
    Serial.println("setRF failed");

  Serial.println("init done");
}

void loop()
{
  if (nrf24.available()) {
    Serial.println("Incoming message intercepted...");
    uint8_t buf[RH_NRF24_MAX_MESSAGE_LEN];
    uint8_t len = sizeof(buf);
    if (nrf24.recv(buf, &len)) {
      int humidity_value = atol((char*)buf);
      Serial.print("humidity_value is ");
      Serial.println(humidity_value);
      Serial.println("");
    } else {
      Serial.println("recv failed, skipping...\n");
    }
 }
}
```

Appendix B

Measurement Equipment Specification

L16 Specifications			
Gearing Option	35:1	63:1	150:1
Peak Power Point	50N @16mm/s	75N @10mm/s	175N @4mm/s
Peak Efficiency Point	24N @24mm/s	38N @15mm/s	75N @7mm/s
Max Speed (no load)	32mm/s	20mm/s	8mm/s
Max Force (lifted)	50N	100N	200N
Back Drive Force	31N	46N	102N
Stroke Option	50mm	100mm	140mm
Mass	56g	74g	84g
Repeatability (-P & LAC)	0.3mm	0.4mm	0.5mm
Max Side Load (extended)	40N	30N	20N
Closed Length (hole to hole)	118mm	168mm	208mm
Feedback Potentiometer	6kΩ±50%	11kΩ±50%	16kΩ±50%
Feedback Linearity	Less than 2.00%		
Input Voltage	0-15 VDC. Rated at 12VDC.		
Stall Current	650mA @ 12V		
Operating Temperature	-10°C to +50°C		
Audible Noise	60dB @ 45cm		
Ingress Protection	IP-54		
Mechanical Backlash	0.25mm		
Limit Switches	Max. Current Leakage: 8uA		
Maximum Static Force	250N		
Maximum Duty Cycle	20%		

Figure B.1: L16 35:1 Linear Actuator Specifications

Rated Output (R.O.):	1 mV/V nominal
Nonlinearity:	0.05% of R.O.
Hysteresis:	0.05% of R.O
Nonrepeatability:	0.05% of R.O.
Zero Balance:	3.0% of R.O.
Compensated Temp. Range:	60° to 160°F
Safe Temp. Range:	-65° to 200°F
Temp. Effect on Output:	0.005% of Load/°F
Temp. Effect on Zero:	0.005% of R.O./°F
Terminal Resistance:	350 ohms nominal
Excitation Voltage:	10 VDC
Safe Overload:	150% of R.O.
Deflection Inches:	0.004 @ R.O.
Weight:	1 oz all ranges
Calibration Included:	Compression
Optional Calibration:	Tension

Dimensions in Inches, GSO-10 through 1000

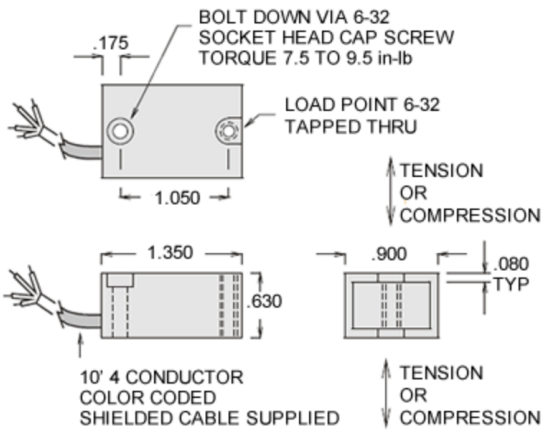

Model	Capacity Grams	Natural Ringing Frequency Hz	Deflection Inches
GSO-10	10	260	0.004
GSO-25	25	475	0.004
GSO-30	30	360	0.004
GSO-50	50	440	0.004
GSO-100	100	610	0.004
GSO-150	150	700	0.004
GSO-250	250	1000	0.004
GSO-500	500	1450	0.004
GSO-1K	1,000	2000	0.004

Figure B.2: GSO-500 Load Cell Specifications

Bibliography

[1] Evan Ackerman. Minirhex makes wiggly-legged unstoppability tiny and affordable, Sep 2023. URL https://spectrum.ieee.org/minirhex-makes-wigglylegged-unstoppability-tiny-and-affordable. 1.1, 1.2

[2] Aditya Balasubramanian, Mike Standish, and Christopher J. Bettinger. Microfluidic thermally activated materials for rapid control of macroscopic compliance. *Advanced Functional Materials*, 24(30):4860–4866, 2014. doi: https://doi.org/10.1002/adfm.201304037. URL https://onlinelibrary.wiley.com/doi/abs/10.1002/adfm.201304037. 1.3.3

[3] Monica Barragan, Nikolai Flowers, and Aaron M. Johnson. Minirhex: A small, open-source, fully programmable walking hexapod, 2018. https://www.andrew.cmu.edu/user/amj1/papers/RSS2018ws_MiniRHex.pdf. 1.2, 1.3.4, 3.2.2

[4] R. Blickhan and R.J. Full. Similarity in multilegged locomotion: Bouncing like a monopode. *Journal of Comparative Physiology A*, 173(5), 1993. doi: 10.1007/bf00197760. 1.3.4, 3.2.2, 3.2.2, 4.3

[5] Bryan Bush, L Wiley Nifong, Hazaim Alwair, and W Randolph Chitwood. Robotic mitral valve surgery-current status and future directions, Nov 2013. URL https://www.ncbi.nlm.nih.gov/pmc/articles/PMC3856989/. 1.3.1

[6] Jeffrey R. Capadona, Kadhiravan Shanmuganathan, Dustin J. Tyler, Stuart J. Rowan, and Christoph Weder. Stimuli-responsive polymer nanocomposites inspired by the sea cucumber dermis. *Science*, 319(5868):1370–1374, 2008. doi: 10.1126/science.1153307. URL https://www.science.org/doi/abs/10.1126/science.1153307. 1.3.3

[7] Ragesh Chellattoan and Gilles Lubineau. A stretchable fiber with tunable stiffness for programmable shape change of soft robots. *Soft Robotics*, 9(6):1052–1061, 2022. doi: 10.1089/soro.2021.0032. URL https://doi.org/10.1089/soro.2021.0032. PMID: 35049362. 1.3.2, 1.3.3

[8] Chao Cheng, Jun Fu, Hang Su, and Luquan Ren. Recent advancements in agriculture robots: Benefits and challenges. *Machines*, 11(1):48, Jan 2023.

ISSN 2075-1702. doi: 10.3390/machines11010048. URL http://dx.doi.org/10.3390/machines11010048. 1.3.1

[9] Nadia G. Cheng, Arvind Gopinath, Lifeng Wang, Karl Iagnemma, and Anette E. Hosoi. Thermally tunable, self-healing composites for soft robotic applications. *Macromolecular Materials and Engineering*, 299(11):1279–1284, 2014. doi: https://doi.org/10.1002/mame.201400017. URL https://onlinelibrary.wiley.com/doi/abs/10.1002/mame.201400017. 1.3.3

[10] Matteo Cianchetti, Alessia Licofonte, Maurizio Follador, Francesco Rogai, and Cecilia Laschi. Bioinspired soft actuation system using shape memory alloys. *Actuators*, 3(3):226–244, 2014. ISSN 2076-0825. doi: 10.3390/act3030226. URL https://www.mdpi.com/2076-0825/3/3/226. 1.3.2, 1.3.3

[11] Alessandro Crespi, Konstantinos Karakasiliotis, Andre Guignard, and A.J. Ijspeert. Salamandra robotica ii: An amphibious robot to study salamander-like swimming and walking gaits. *Robotics, IEEE Transactions on*, 29:308–320, 04 2013. doi: 10.1109/TRO.2012.2234311. 1.3.2

[12] Daniel Koditschek Daniel Goldman, Haldun Komsuoglu. March of the sandbots, 2009. https://shorturl.at/dFLX3. 1.3.4

[13] Weiqiang Dou, Guoliang Zhong, Jinglin Cao, Zhun Shi, Bowen Peng, and Liangzhong Jiang. Soft robotic manipulators: Designs, actuation, stiffness tuning, and sensing. *Advanced Materials Technologies*, 6(9), 2021. doi: 10.1002/admt.202100018. 1.3.3

[14] Magnus Egerstedt and Jonathan Pauli. The slothbot: An ecologically inspired environmental monitoring robot. *Edentata: The Newsletter of the IUCN/SSC Anteater, Sloth and Armadillo Specialist Group*, 2020. doi: 10.2305/iucn.ch.2020.edentata-20-1.7.en. 1.3.1

[15] Kevin C. Galloway, Jonathan E. Clark, Mark Yim, and Daniel E. Koditschek. Experimental investigations into the role of passive variable compliant legs for dynamic robotic locomotion. In *2011 IEEE International Conference on Robotics and Automation*, pages 1243–1249, 2011. doi: 10.1109/ICRA.2011.5979941. 1.3.2, 1.3.4, 1.3.4, 4

[16] Farhan Gandhi and Sang-Guk Kang. Beams with controllable flexural stiffness. *Smart Materials and Structures*, 16(4):1179, jun 2007. doi: 10.1088/0964-1726/16/4/028. URL https://dx.doi.org/10.1088/0964-1726/16/4/028. 1.3.3

[17] C. Georgiades, A. German, A. Hogue, Hui Liu, C. Prahacs, A. Ripsman, R. Sim, L.-A. Torres, Pifu Zhang, M. Buehler, G. Dudek, M. Jenkin, and E. Milios. Aqua: an aquatic walking robot. In *2004 IEEE/RSJ International Conference on Intelligent Robots and Systems (IROS) (IEEE Cat. No.04CH37566)*, volume 4, pages 3525–3531 vol.4, 2004. doi: 10.1109/IROS.2004.1389962. 1.1, 1.3.4

[18] Robert Grabowski, Luis E. Navarro-Serment, and Pradeep K. Khosla. An army of small robots. *Scientific American*, 289(5):62–67, 2003. ISSN 00368733, 19467087. URL http://www.jstor.org/stable/26060527. 1.3.1

[19] Wenqi Hu, Guo Zhan Lum, Massimo Mastrangeli, and Metin Sitti. Small-scale soft-bodied robot with multimodal locomotion. *Nature*, 554(7690):81–85, 2018. doi: 10.1038/nature25443. 1.3.2

[20] Di Shun Huang, Jian Hu, Liuchunzi Guo, Yi Sun, and Liao Wu. A static model for a stiffness-adjustable snake-like robot. In *2021 IEEE/RSJ International Conference on Intelligent Robots and Systems (IROS)*, pages 2956–2961, 2021. doi: 10.1109/IROS51168.2021.9636734. 1.3.2

[21] Eric Jaffe. Walking on water: Tree frog's foot uses dual method to stick, Jun 2006. https://www.sciencenews.org/article/walking-water-tree-frogs-foot-uses-dual-method-stick. 1.3.2

[22] Haidar Jamal. Localization for lunar micro-rovers, 2021. https://www.ri.cmu.edu/app/uploads/2021/05/Haidar_Jamal_Thesis.pdf. 1.3.1

[23] Yong-Jae Kim, Shanbao Cheng, Sangbae Kim, and Karl Iagnemma. A stiffness-adjustable hyperredundant manipulator using a variable neutral-line mechanism for minimally invasive surgery. *IEEE Transactions on Robotics*, 30(2):382–395, 2014. doi: 10.1109/TRO.2013.2287975. 1.3.1

[24] Jennifer Kite-Powell. Tiny bio-inspired robot modeled from feet of a tree frog, Jun 2013. URL https://www.forbes.com/sites/jenniferhicks/2013/06/08/tiny-bio-inspired-robot-modeled-from-feet-of-a-tree-frog/?sh=319c98e81720. 1.3.2

[25] Haldun Komsuoglu, Anirudha Majumdar, Yasemin Ozkan Aydin, and Daniel Koditschek. Characterization of dynamic behaviors in a hexapod robot. *Springer Tracts in Advanced Robotics*, 79, 12 2010. doi: 10.1007/978-3-642-28572-1_46. 1.3.4

[26] Roy Kornbluh, Ron Pelrine, and Joe Eckerle. Chapter 22 - application to very small devices: Microactuators, micro-optics, microfluidics, and more. In Federico Carpi, Danilo De Rossi, Roy Kornbluh, Ronald Pelrine, and Peter Sommer-Larsen, editors, *Dielectric Elastomers as Electromechanical Transducers*, pages 227–238. Elsevier, Amsterdam, 2008. ISBN 978-0-08-047488-5. doi: https://doi.org/10.1016/B978-0-08-047488-5.00022-8. URL https://www.sciencedirect.com/science/article/pii/B9780080474885000228. 1.3.1

[27] Cecilia Laschi, Matteo Cianchetti, Barbara Mazzolai, Laura Margheri, Maurizio Follador, and Paolo Dario. Soft robot arm inspired by the octopus. *Advanced Robotics*, 26(7):709–727, 2012. doi: 10.1163/156855312X626343. URL https://doi.org/10.1163/156855312X626343. 1.3.2

[28] Cecilia Laschi, Barbara Mazzolai, and Matteo Cianchetti. Soft robotics: Technologies and systems pushing the boundaries of robot abilities. *Science Robotics*, 1(1):eaah3690, 2016. doi: 10.1126/scirobotics.aah3690. URL https://www.science.org/doi/abs/10.1126/scirobotics.aah3690. 1.3.2, 1.3.3

[29] Chen Li, Paul B. Umbanhowar, Haldun Komsuoglu, Daniel E. Koditschek, and Daniel I. Goldman. Sensitive dependence of the motion of a legged robot on granular media. *Proceedings of the National Academy of Sciences*, 106(9):3029–3034, 2009. doi: 10.1073/pnas.0809095106. URL https://www.pnas.org/doi/abs/10.1073/pnas.0809095106. 1.3.4

[30] Pedersen S. M., Fountas S., and Blackmore S. Agricultural robots; applications and economic perspectives. In Yoshihiko Takahashi, editor, *Service Robot Applications*, chapter 21. IntechOpen, Rijeka, 2008. doi: 10.5772/6048. URL https://doi.org/10.5772/6048. 1.3.1

[31] Nima Mahkam, Alihan Bakir, and Onur Özcan. Miniature modular legged robot with compliant backbones. *IEEE Robotics and Automation Letters*, 5(3):3923–3930, 2020. doi: 10.1109/LRA.2020.2982362. 1.3.1

[32] Spencer J. Matonis, Bozhong Zhuang, Ailla F. Bishop, Durva A. Naik, Zeynep Temel, and Christopher J. Bettinger. Edible origami actuators using gelatin-based bioplastics. *ACS Applied Polymer Materials*, 5(8):6288–6295, 2023. doi: 10.1021/acsapm.3c00919. URL https://doi.org/10.1021/acsapm.3c00919. 1.2, 2, 2.2.1, 2.2.3

[33] Barbara Mazzolai, Alessio Mondini, Francesca Tramacere, Gianluca Riccomi, Ali Sadeghi, Goffredo Giordano, Emanuela Del Dottore, Massimiliano Scaccia, Massimo Zampato, and Stefano Carminati. Octopus-inspired soft arm with suction cups for enhanced grasping tasks in confined environments. *Advanced Intelligent Systems*, 1(6):1900041, 2019. doi: https://doi.org/10.1002/aisy.201900041. URL https://onlinelibrary.wiley.com/doi/abs/10.1002/aisy.201900041. 1.3.2

[34] M Andy McEvoy and Nikolaus Correll. Thermoplastic variable stiffness composites with embedded, networked sensing, actuation, and control. *Journal of Composite Materials*, 49(15):1799–1808, 2015. doi: 10.1177/0021998314525982. URL https://doi.org/10.1177/0021998314525982. 1.3.3

[35] Geoffrey Mcknight, Robert Doty, Andrew Keefe, Guillermo Herrera, and Chris Henry. Segmented reinforcement variable stiffness materials for reconfigurable surfaces. *Journal of Intelligent Material Systems and Structures*, 21(17):1783–1793, 2010. doi: 10.1177/1045389X10386399. URL https://doi.org/10.1177/1045389X10386399. 1.3.3

[36] Brian Mertins. How does environment affect animal behavior?, 2023. https://shorturl.at/dFOP6. 1.1

[37] Tiana Miller-Jackson, Yi Sun, Rainier Natividad, and Chen Hua Yeow. Tubular jamming: A variable stiffening method toward high-force applications with soft robotic components. *Soft Robotics*, 6(4):468–482, 2019. doi: 10.1089/soro.2018.0084. URL https://doi.org/10.1089/soro.2018.0084. PMID: 31158061. 1.3.3

[38] Lars Pfotzer, Steffen Ruehl, Georg Heppner, Arne Roennau, and Rüdiger Dillmann. Kairo 3: A modular reconfigurable robot for search and rescue field missions. In *2014 IEEE International Conference on Robotics and Biomimetics, IEEE ROBIO 2014*, 12 2014. doi: 10.1109/ROBIO.2014.7090331. 1.3.1

[39] Zeeshan Qaiser, Liping Kang, and Shane Johnson. Design of a bioinspired tunable stiffness robotic foot. *Mechanism and Machine Theory*, 110:1–15, 2017. ISSN 0094-114X. doi: https://doi.org/10.1016/j.mechmachtheory.2016.12.003. URL https://www.sciencedirect.com/science/article/pii/S0094114X1630653X. 1.3.2

[40] Uluc. Saranli, Martin Buehler, and Daniel E. Koditschek. Rhex: A simple and highly mobile hexapod robot, July 2001. URL https://www.ri.cmu.edu/pub_files/pub4/saranli_uluc_2001_1/saranli_uluc_2001_1.pdf. 1.1

[41] Uluc Saranli, Martin Buehler, and Daniel E. Koditschek. Rhex: A simple and highly mobile hexapod robot. *The International Journal of Robotics Research*, 20(7):616–631, 2001. doi: 10.1177/02783640122067570. URL https://doi.org/10.1177/02783640122067570. 1.1

[42] Jenna Seetohul and Mahmood Shafiee. Snake robots for surgical applications: A review. *Robotics*, 11(3), 2022. ISSN 2218-6581. doi: 10.3390/robotics11030057. URL https://www.mdpi.com/2218-6581/11/3/57. 1.3.1

[43] Yu Shan, Yanzhi Zhao, Changlei Pei, Hongnian Yu, and Pengcheng Liu. A novel design of a passive variable stiffness soft robotic gripper. *Bioinspiration & Biomimetics*, 17(6):066014, oct 2022. doi: 10.1088/1748-3190/ac965a. URL https://dx.doi.org/10.1088/1748-3190/ac965a. 1.3.3

[44] Matthew Shen, Angus B. Clark, and Nicolas Rojas. A scalable variable stiffness revolute joint based on layer jamming for robotic exoskeletons. In Abdelkhalick Mohammad, Xin Dong, and Matteo Russo, editors, *Towards Autonomous Robotic Systems*, pages 3–14, Cham, 2020. Springer International Publishing. ISBN 978-3-030-63486-5. 1.3.3

[45] O. Spykman, A. Gabriel, M. Ptacek, and M. Gandorfer. Farmers' perspectives on field crop robots – evidence from bavaria, germany. *Computers and Electronics in Agriculture*, 186:106176, 2021. ISSN 0168-1699. doi: https://doi.org/10.

1016/j.compag.2021.106176. URL https://www.sciencedirect.com/science/article/pii/S0168169921001939. 1.3.1

[46] R. Wood, S. Avadhanula, Ranjana Sahai, E. Steltz, and R. Fearing. Microrobot design using fiber reinforced composites. *Journal of Mechanical Design - J MECH DESIGN*, 130, 05 2008. doi: 10.1115/1.2885509. 2.1

[47] Milan Yogendrappa. Fr4 material for pcb fabrication, July 2021. URL https://www.protoexpress.com/blog/why-fr4-material-in-pcb-fabrication/. 2.1.5

[48] Samuel M. Youssef, MennaAllah Soliman, Mahmood A. Saleh, Mostafa A. Mousa, Mahmoud Elsamanty, and Ahmed G. Radwan. Underwater soft robotics: A review of bioinspiration in design, actuation, modeling, and control. *Micromachines*, 13(1):110, 2022. doi: 10.3390/mi13010110. 1.3.1

[49] HAO Yufei, WANG Tianmiao, FANG Xi, and WEN Li. A variable stiffness soft robotic gripper with low-melting-point alloy, 2017. https://softrobotics.buaa.edu.cn/Download/2017/2017-CCC-Haoyufei.pdf. 1.3.3

[50] Yuan-Fang Zhang, Ningbin Zhang, Hardik Hingorani, Ningyuan Ding, Dong Wang, Chao Yuan, Biao Zhang, Guoying Gu, and Qi Ge. Fast-response, stiffness-tunable soft actuator by hybrid multimaterial 3d printing. *Advanced Functional Materials*, 29(15):1806698, 2019. doi: https://doi.org/10.1002/adfm.201806698. URL https://onlinelibrary.wiley.com/doi/abs/10.1002/adfm.201806698. 1.3.3

[51] Xinyuan Zhao, Yuqiang Wu, Yangwei You, Arturo Laurenzi, and Nikos Tsagarakis. Variable stiffness locomotion with guaranteed stability for quadruped robots traversing uneven terrains. *Frontiers in Robotics and AI*, 9, 2022. doi: 10.3389/frobt.2022.874290. 1.3.2

[52] Q. Zhong, J. Zhu, F. E. Fish, S. J. Kerr, A. M. Downs, H. Bart-Smith, and D. B. Quinn. Tunable stiffness enables fast and efficient swimming in fish-like robots. *Science Robotics*, 6(57):eabe4088, 2021. doi: 10.1126/scirobotics.abe4088. URL https://www.science.org/doi/abs/10.1126/scirobotics.abe4088. 1.3.2

[53] Yong Zhong, Ruxu Du, Liao Wu, and Haoyong Yu. A novel articulated soft robot capable of variable stiffness through bistable structure. In *2020 IEEE International Conference on Robotics and Automation (ICRA)*, pages 2939–2945, 2020. doi: 10.1109/ICRA40945.2020.9197479. 1.3.2